ANALYSIS AND DESIGN OF DUAL-POLARIZED WIDEBAND PATCH
ANTENNAS ELECTROMAGNETICALLY EXCITED WITH ELEVATED
WIDE STRIPS

A THESIS SUBMITTED TO
THE GRADUATE SCHOOL OF NATURAL AND APPLIED SCIENCES
OF
MIDDLE EAST TECHNICAL UNIVERSITY

BY

ADİL FIRAT YILMAZ

IN PARTIAL FULFILLMENT OF THE REQUIREMENTS
FOR
THE DEGREE OF MASTER OF SCIENCE
IN
ELECTRICAL AND ELECTRONICS ENGINEERING

FEBRUARY 2014

Approval of the thesis:

ANALYSIS AND DESIGN OF DUAL-POLARIZED WIDEBAND PATCH ANTENNAS ELECTROMAGNETICALLY EXCITED WITH ELEVATED WIDE STRIPS

submitted by **ADİL FIRAT YILMAZ** in partial fulfillment of the requirements for the degree of **Master of Science in Electrical and Electronics Engineering Department, Middle East Technical University** by,

Prof. Dr. Gülbin Dural Ünver
Dean, Graduate School of **Natural and Applied Sciences** _____

Prof. Dr. Gönül Turhan Sayan
Head of Department, **Electrical and Electronics Eng.** _____

Assoc. Prof. Dr. Lale Alatan
Supervisor, **Electrical and Elect. Eng. Dept., METU** _____

Examining Committee Members:

Prof. Dr. Sencer KOÇ
Electrical and Electronics Engineering Dept., METU _____

Assoc. Prof. Dr. Lale Alatan
Electrical and Electronics Engineering Dept., METU _____

Prof. Dr. Altunkan Hızal
Electrical and Electronics Engineering Dept., METU _____

Prof. Dr. Özlem Aydın Çivi
Electrical and Electronics Engineering Dept., METU _____

Nihan Öznazlı, M.Sc.
Senior Expert Engineer, ASELSAN Inc. _____

Date: 05.02.2015

I hereby declare that all information in this document has been obtained and presented in accordance with academic rules and ethical conduct. I also declare that, as required by these rules and conduct, I have fully cited and referenced all material and results that are not original to this work.

Name, Last Name: ADİL FIRAT YILMAZ

Signature   :

ABSTRACT

ANALYSIS AND DESIGN OF DUAL-POLARIZED WIDEBAND PATCH
ANTENNAS ELECTROMAGNETICALLY EXCITED WITH ELEVATED
WIDE STRIPS

Yılmaz, Adil Fırat

M.S., Department of Electrical and Electronics Engineering

Supervisor   : Assoc. Prof. Dr. Lale Alatan

February 2014, 63 pages

In communication systems like WiMAX, WLAN, 3G, 4G and LTE, design of wideband and dual polarized antennas are required. It is known that bandwidth of patch antennas can be broaden by using thick air substrates. The bandwidth can be further improved by using three dimensional feed strucutures that are electromagnetically coupled to the patch.

In this thesis, microstrip patch antennas that are excited by elevated wide strips are studied. First, a linearly polarized antenna is considered and the effects of antenna and feed parameters on the input impedance characteristics are investigated through EM simulations. Then a dual polarized antenna is considered and the effects of antenna parameters on the radiation performance (i.e. isolation) is explored. In the light of these observations, guidelines for the design of dual polarized wideband patch antennas excited with elevated wide strips is presented. To demonstrate the usage of these guidelines an antenna, which operates in a different frequency band, is designed by following the steps of the proposed design procedure. Finally, the input impedance and radiation pattern measurements of a two element antenna array that was previously designed as a base station antenna are performed. Simulation and measurement results are compared and discussed. The EM simulations are performed by a Finite

Element based full-wave analysis software HFSS by Ansys.

ÖZ

YÜKSELTİLMİŞ GENİŞ ŞERİTLERLE ELEKTROMANYETİK ŞEKİLDE
UYARILAN ÇİFT KUTUPLU GENİŞ BANT YAMA ANTENLERİN
ANALİZİ VE TASARIMI

Yılmaz, Adil Fırat

Yüksek Lisans, Elektrik ve Elektronik Mühendisliği Bölümü

Tez Yöneticisi   : Doç. Dr. Lale Alatan

WiMAX, WLAN, 3G, 4G ve LTE gibi haberleşme sistemlerinde geniş bantlı ve
çift kutuplu anten tasarımlarına ihtiyaç duyulmaktadır. Bant genişliğini arttır-
mak için anten alt tabakası olarak kalın hava tabakası kullanıldığı bilinmektedir.
Bant genişliği üç boyutlu besleme yapılarının elektromanyetik olarak yama an-
tene bağlaşım yaptırılarak daha da arttırılabilmektedir.

Bu tezde, yükseltilmiş geniş şeritlerle elektromanyetik şekilde uyarılan yama an-
tenler üzerinde çalışılmıştır. İlk olarak doğrusal kutuplu antenler ele alınmış ve
anten ve besleme parametrelerinin giriş özdirenç karakterisğine olan etkileri EM
benzetimleri ile incelenmiştir. Daha sonra çift kutuplu antenler ele alınmış ve
anten parametrelerinin ışınım performansına (izolasyon) etkileri araştırılmıştır.
Bu gözlemlerin ışığında, yükseltilmiş geniş şeritlerle elektromanyetik şekilde uya-
rılan çift kutuplu geniş bant yama antenler için tasarım yönergeleri sunulmutur.
Bu yönergelerin kullanımını göstermek amacıyla önerilen tasarım adımları ile
farklı frekans bandında çalışan bir anten tasarlanmıştır. Son olarak önceden baz
istasyonu için tasarlanmış iki elemanlı dizi anten için giriş özdirenç ve ışınım
örüntü ölçümleri gerçekleştirilmiştir. Benzetim ve ölçüm sonuçları karşılaştırıl-
mış ve tartışılmıştır. EM benzetimleri Sonlu Eleman tabanlı tam dalga analizi
yapabilen Ansys firmasına ait HFSS yazılımı ile gerçekleştirilmiştir.

Anahtar Kelimeler: Geniş Bant, Çift Kutuplu, İstiflenmiş yama, Yükseltilmiş besleme

to my fiancé and my dear family

ACKNOWLEDGEMENTS

TABLE OF CONTENTS

LIST OF TABLES

TABLES

LIST OF FIGURES

FIGURES

LIST OF ABBREVIATIONS

ϵ_r	Relative Permittivity
FDTD	Finite Difference Time Domain
FEM	Finite Element Method
GHz	Giga Hertz
GPS	Global Positioning System
HFSS	High Frequency Structural Simulator
λ	Wavelength
MHz	Mega Hertz
MoM	Method of Moments
UMTS	Universal Mobile Telecommunications System
WiMAX	Worldwide Interoperability for Microwave Access
WLAN	Wireless Local Area Network

CHAPTER 1

INTRODUCTION

Due to the rapid development in the field of satellite and wireless communication there has been a great demand for low cost, light weight, compact, low profile antennas that are capable of maintaining high performance over a large spectrum of frequencies. Many of the antenna applications for satellite links, mobile communications, and wireless local-area networks, impose constraints on compactness, dual frequency operation, frequency agility, polarization control, and radiation control. Compact microstrip antennas capable of dual polarized radiation are very suitable for applications in wireless communication systems that demand frequency reuse and polarization diversity[5]. As shown in Fig. 1.1, a microstrip antenna in its simplest configuration consists of a radiating patch on one side of a dielectric substrate and a ground plane on the other side. The patch conductors normally made of copper or gold, can assume virtually any shape, but regular shapes, such as rectangles and circles, are generally used to easily predict the performance of the antenna by using simple analytical methods. In literature, there are numerous type of substrates ($2.2 \leq \epsilon_r \leq 12$) that can be used to design microstrip antennas.

Early microstrip antennas were fed either by a microstrip line or a coaxial probe through the ground plane. There are lots of ways that can be used to feed microstrip patch antennas. These methods can be classified into two categories, contacting and non-contacting. In the contacting method, the RF power is fed directly to the radiating patch using a connecting element such as a microstrip line or a coaxial probe. In contacting microstrip line feeding, both the patch
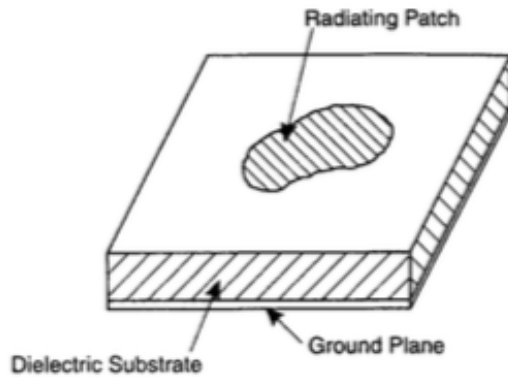
Figure 1.1: Microstrip Patch Antenna Configuration

and the line are located on the same substrate. In coaxial probe feed, the inner conductor of the coaxial line is attached to the radiating patch while the outer conductor is connected to the ground plane. Both the microstrip line feed and the coaxial probe feed have inherent asymmetries which generate higher order modes that produce cross-polarized radiation. To overcome some of these problems, non-contacting feeding schemes are introduced. In the non-contacting scheme, electromagnetic field coupling is used to transfer power between the microstrip line and the radiating patch, which are printed on different dielectric substrates. The most popular ones are the aperture coupled (or slot coupled), and proximity coupled (or electromagnetically coupled) patches. The aperture coupling consists of two substrates separated by a ground plane. On the bottom side of the lower substrate there is a microstrip feed line whose energy is coupled to the patch through a slot on the ground plane between the two substrates.

A rectangular or circular patch antenna with a single feed provides linear polarization or circular polarization through some perturbations in the shape of the antenna. Dual polarization can be achieved by two orthogonal feeds.

Microstrip patch antennas are preferred when the issues like ease of manufacturing, low cost, ease of integration and ease of forming arrays are considered. On the other hand, when evaluating the use of microstrip patch antennas, one should be aware of their disadvantages like impedance bandwidth limitations, excitation of surface waves and radiation performance limits.

2

Narrow impedance bandwidth is one of the most problematic issue for microstrip patch antennas. In order to increase impedance bandwidth, thicker substrates with low dielectric constant should be used to enhance the fringing fields that account for radiation. A microstrip structure with the line and the patch on the same level cannot be optimized simultaneously as an antenna or as a transmission line because the specific requirements for both are contradictory. A low dielectric constant is needed for the efficient radiation from the patch. However, it will result in spurious radiation from line and step discontinuities. To reduce the radiation from the microstrip line if we use high dielectric constant substrate, it will degrade the radiation efficiency of the patch and increase the surface wave loss. Therefore, non-contacting feeding structures which allow independent optimization of the feed mechanism and the radiating element should be preferred in the design of microstrip antennas. Typically, a dielectric material with high permittivity is used for the feed substrate, and thick low dielectric constant material for the antenna substrate. In slot-coupled microstrip antennas the bandwidth can be further increased by tuning additional resonance introduced by the slot close to the resonance of the patch. By using slot-coupled feeding technique bandwidths on the order of %30-35 can be achieved for single polarization [6] [7]. However, as the thickness of the antenna substrate is increased to increase the bandwidth, the length of the slot becomes larger to achieve proper coupling. Depending on the required bandwidth, the design of the dual polarized antennas may become impossible due to difficulties associated with positioning two orthogonal long slots. To eliminate this problem, the use of slot shapes other than rectangular is proposed. In [8] dual polarized antennas with %20 bandwidth are designed by using H-shaped slots. When larger bandwidths are required, low isolation between orthogonal ports starts to be a problem. Hence other feeding techniques should be explored for the design of dual polarized wide band antennas.

When bandwidths as large as %40-50 are required conventional proximity coupled feeding structures are not suitable candidates either. Because, as the thickness of the antenna substrates increases the coupling between the microstrip line and the patch becomes weaker, and the antenna cannot be excited efficiently.

3

Consequently, coaxial probe feeding is left as sole alternatives. However, for this choice, the input impedance matching becomes problematic due to the high inductance introduced by the long probe required for the thick substrate. Hence some modifications in the shape of the feed probe is proposed to decrease this inductive effect. One of these modifications is bending the probe in L-shape or T-shape as shown in Fig. 1.2, to compensate the high inductance of the long probe with the capacitance associated with the electromagnetic coupling between the probe and the antenna. A dual polarized antenna with L-shaped probe feed is proposed in [9] and %23.8 bandwidth is achieved.
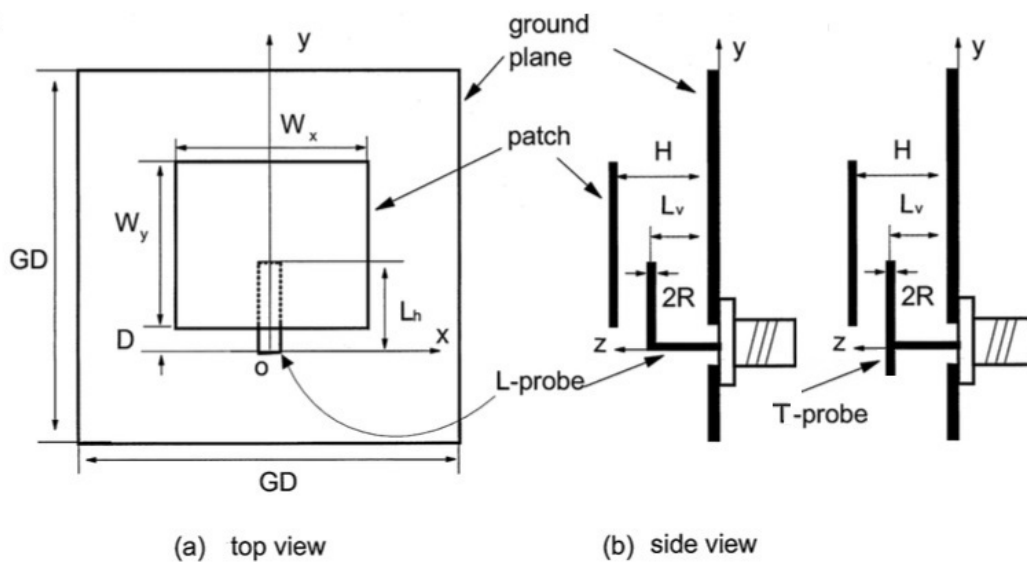
Figure 1.2: L-shaped and T-shaped Probe Feeds [1]

Another alternative for modifying the shape of the probe feed was proposed by Herscovici [3]. He demonstrated that %64 bandwidth (2.2 GHz - 4.3 GHz, almost octave bandwidth) can be obtained by using wide metallic strips instead of a thin inner conductor of the probe as shown in Fig.1.3.
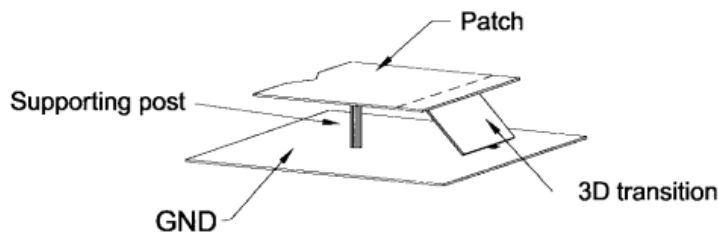
Figure 1.3: 3D Transmission Line Feed Model, Herscovici Design [2]

However, another problem arises when the bandwidth of the antenna starts to approach octave band. When the cavity model is considered the dominant mode of the antenna is TM_{10} mode, which results in broadside radiation. As the frequency approaches to twice the operating frequency of this mode TM_{20} mode starts to be excited which results in a null in near broadside direction, Fig.1.4. Hence, even though a large impedance bandwidth is obtained, the antenna cannot be considered wide band due to this deficiency in radiation characteristics.
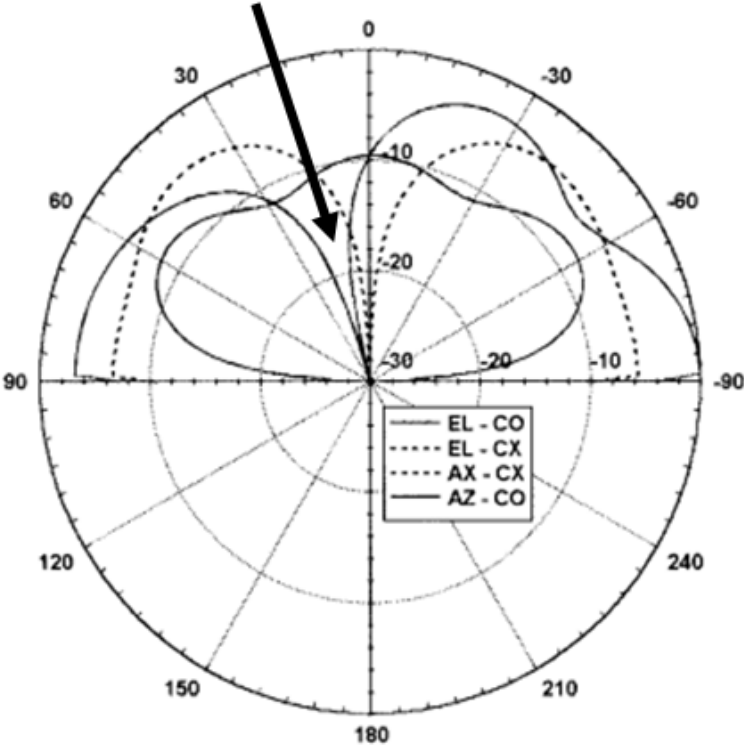
Figure 1.4: Radiation Pattern at 4.7 GHz in [3]

Recently, a different feeding structure is proposed by Hızal [4], that combines the advantages of two aforementioned feeding techniques. As shown in Fig.1.5, the proposed feeding structure is an L-shaped wide strip. The L-shaped electromagnetically coupled feed proposed in [1] is combined with the wide strip proposed in [3], and consequently wide strip L-shaped feeding structure is formed. The main advantage of this feeding structure is the radiation due to the feed structure. As it will be demonstrated in the following chapters, the radiation from the feed eliminates the null at the near broadside direction occurring for TM_{20}

mode.
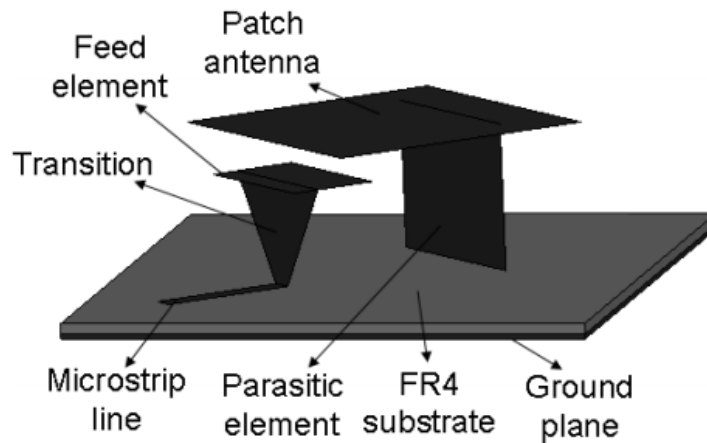
Figure 1.5: L-shaped Wide Strip [4]

In this study, with the contributions of all information given previously, analysis and design of a dual-polarized wideband patch antenna which is electromagnetically excited with elevated wide strips are presented. The effects of antenna parameters on the input impedance and radiation performance of the antenna is studied through parametric analysis. During the analysis of dual polarized antennas the cross-polarization of the orthogonal ports is also considered as a performance measure. Besides, an explanatory guideline is also introduced in order to guide antenna engineers during the design of similar antennas. Additionally, previously designed and manufactured two-element array consisting of dual polarized stacked patch antennas is simulated and measured. Comparison of simulation and measurement results are presented and discussed. Antenna characteristics like impedance bandwidth, return loss and port isolation are all analyzed with a finite element based EM simulation tool HFSS by ANSYS.

Chapter 2 provides simulation results and discussions for parametric analysis are also presented. A design procedure for wideband patch antennas proximity coupled with elevated wide strips is introduced. An application of the introduced design guidelines is provided through a design example at a different frequency band.

Chapter 3 includes simulation results of the dual polarized structure and corresponding comments on newly introduced port and isolation issues due to the

second port.

Chapter 4 compares simulation and measurement results of a two element array of proximity coupled dual polarized stacked patch antennas. The effects of stacked patches on the input impedance bandwidth and isolation of the antenna are discussed.

Chapter 5 summarizes all the important observations and results from previous chapters.

CHAPTER 2

SIMULATIONS AND RESULTS FOR SINGLE FEED SINGLE PATCH CONFIGURATION

In this chapter, we provide an example in order to demonstrate the ability of designing wideband electromagnetically coupled patch antenna. In order to show the effects of parameters used during the design procedure, a single patch with a single elevated electromagnetically coupled feed configuration is studied. All the analysis is done in ANSYS HFSS simulation software.

In the first part, the characteristics of an elevated wide strip and maximum impedance bandwidth with this feed and single patch antenna are introduced. Then the effects of parameters on a single patch antenna electromagnetically excited with an elevated wide strip are observed. In this configuration, guidelines for single patch design are introduced.

In the second part, an example of a demonstration of guidelines that are given in the following sections is presented by transforming the design from 1.5 GHz - 2.5 GHz band to 3 GHz - 5 GHz band. The steps used during this transformation is explained and corresponding results are presented and discussed.

2.1 Analysis and Design of a Single Rectangular Patch with a Single Electromagnetically Coupled Feed

In this section, parametric analysis of a single rectangular patch antenna with a single electromagnetically coupled feed is given. Structure and parameters of

the antenna are shown in Fig. 2.1. To be noted that, in order to provide a good visibility of the antenna structure, the ground plane and the dielectric substrate is removed.
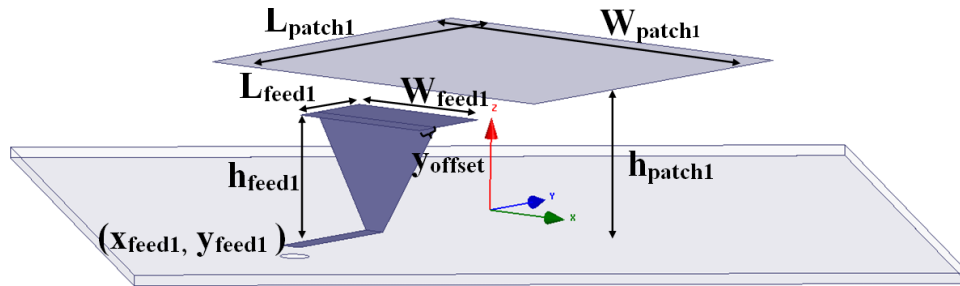
Figure 2.1: Structure and Parameters of a Single Rectangular Patch with a Single Electromagnetically Coupled Feed

To estimate the initial dimensions for the patch antenna cavity model is utilized.
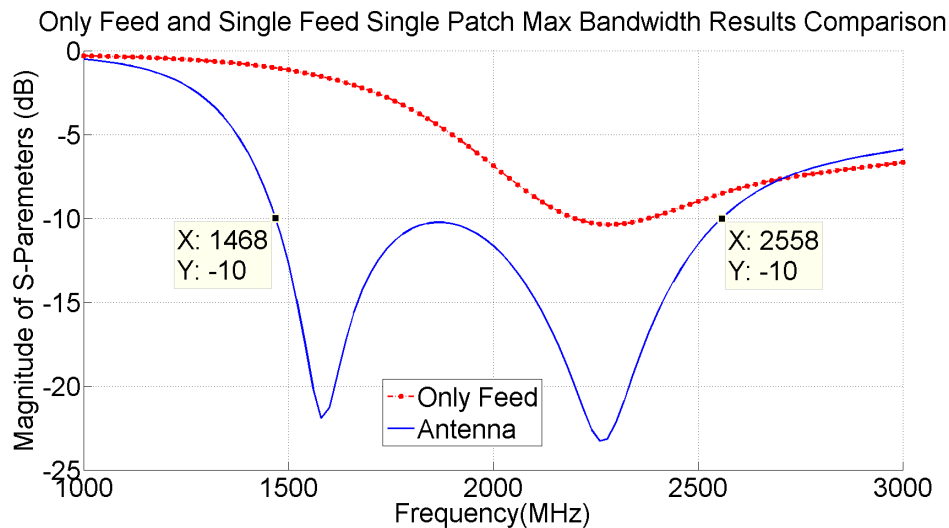
Figure 2.2: Only Feed and Single Rectangular Patch with a Single Electromagnetically Coupled Feed S_{11} Characteristics

The antenna proposed in [4] is optimized through a couple of HFSS analysis to obtain the best possible input impedance bandwidth. The input return loss of the optimized antenna is shown in Fig.2.2 (solid blue line). The antenna provides a %54 bandwidth between 1.468 GHz and 2.558 GHz. The corresponding design parameters which maximize the impedance bandwidth are given in Table 2.1. Then to better understand the radiation mechanism and the double resonance behavior of this wideband antenna the feed structure is analyzed without the patch antenna and the results are also presented in Fig.2.2 (dashed red line) for

comparison. From Fig.2.2 it can be observed that the resonance around 2.3 GHz is due to the feed structure. In order to explore whether the resonance around 1.6 GHz belongs to the patch or not, the cavity model is utilized to estimate the resonance frequency of the patch only. In this model the microstrip antenna is modeled as a cavity bounded by electric walls at top and the bottom, and magnetic walls at side peripheries. In this analytical model it is assumed that the antenna substrate is very thin with respect to wavelength, such that the electric field does not change along z-direction. With this assumption the boundary value problem is solved and the resonance frequency of a cavity mode is given as [10]:

$$(f_r)_{mn} = \frac{1}{2\pi\sqrt{\mu\epsilon}}\sqrt{\left(\frac{m\pi}{L_{patch}}\right)^2 + \left(\frac{n\pi}{W_{patch}}\right)^2} \qquad (2.1)$$

When the feed is located at the center of the edge along x-direction as shown in Fig.2.1, the resonance frequency of the fundamental mode (TM_{10}) becomes

$$\begin{aligned}
(f_r)_{10} &= \frac{1}{2\pi\sqrt{\mu\epsilon}}\sqrt{\left(\frac{\pi}{L_{patch}}\right)^2} \\
&= \frac{c}{2L_{patch}\sqrt{\epsilon_r}}
\end{aligned} \qquad (2.2)$$

where c is the speed of light in free space, ϵ_r is the dielectric constant of the substrate. Even though the peripheral of the patch is assumed to be PMC, in practice, fringing fields occur. Therefore, the length of the patch needs to be extended by ΔL to account for these fringing fields. Moreover, since the dielectric medium does not extend above the patch, effective dielectric constant (ϵ_{reff}) of the geometry should be used instead of ϵ_r. Hence Eq.2.2 takes the following form with the above corrections.

$$(f_r)_{10} = \frac{c}{2(L_{patch} + 2\Delta L_{patch})\sqrt{\epsilon_{reff}}} \qquad (2.3)$$

ΔL and ϵ_{reff} can be calculated by using the following formulas[10].

11

$$\frac{\Delta L_{patch}}{h_{patch}} = 0.412 \frac{(\epsilon_{reff} + 0.3)\left(\dfrac{W_{patch}}{h_{patch}} + 0.264\right)}{(\epsilon_{reff} - 0.258)\left(\dfrac{W}{h} + 0.8\right)} \tag{2.4}$$

$$\frac{W_{patch}}{h_{patch}} > 1$$

$$\epsilon_{reff} = \frac{\epsilon_r + 1}{2} + \frac{\epsilon_r - 1}{2}\left[1 + 12\frac{h_{patch}}{W_{patch}}\right]^{-1/2} \tag{2.5}$$

For this optimized design L_{patch}=57mm, h_{patch}=21.4mm, since the antenna uses air substrate ϵ_{reff}=1. Hence by using Eq.2.3 the resonance frequency of the patch calculated to be 1.5 GHz. Consequently, the resonant frequencies around 1.6 GHz and 3.3 GHz are considered to be associated with the radiating patch and elevated feed respectively.

In addition to impedance bandwidth analysis, co-polarization and cross-polarization characteristics of the optimum design are presented in Fig. 2.3 and 2.4 for two principal planes, ϕ=0° and ϕ=90° respectively.

If we compare the patterns at Fig. 2.3a and 2.3b, it can be observed that as frequency changes from 1500 MHz to 2300 MHz, the cross-polarized field levels increase. This observation supports the claim that the resonance around 2.3 GHz is due to the feed structure. Because the feed structure may be considered as a top-loaded monopole and the far field of this monopole is expected to exhibit a similar characteristic as the blue lines Fig. 2.3. Hence, the contribution of the cross-polarized field increases as we approach to the resonance frequency of the feed. At ϕ=90° plane, due to the huge difference between co-pol/cross-pol levels and the range of the graphs in Fig.2.4 are also very large (70 dB). In order to make a better comparison of the co-polarized field patterns at two different frequencies, they are presented on the same graph(Fig.2.5) with smaller scale (30 dB) to observe small changes. According to Fig. 2.5, it is observed that a null like drop (-17 dB) occurs at 40°.This is probably due to the out-of-phase cancellation of the radiated fields from the patch and feed structure. In order to investigate whether a null occurs at the near broadside direction

12
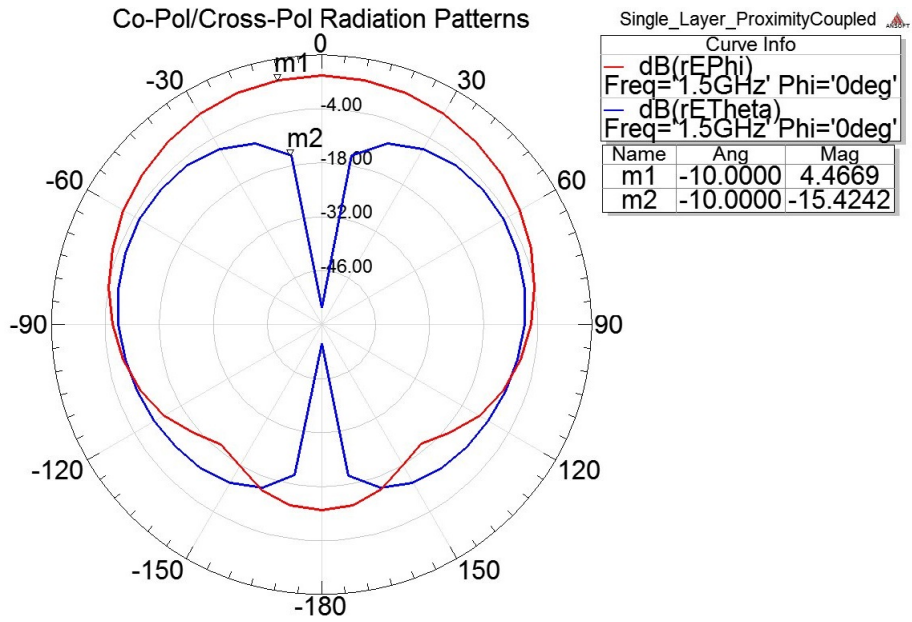
(a) Co-Pol/Cross-Pol for 1500 MHz at $\phi=0°$
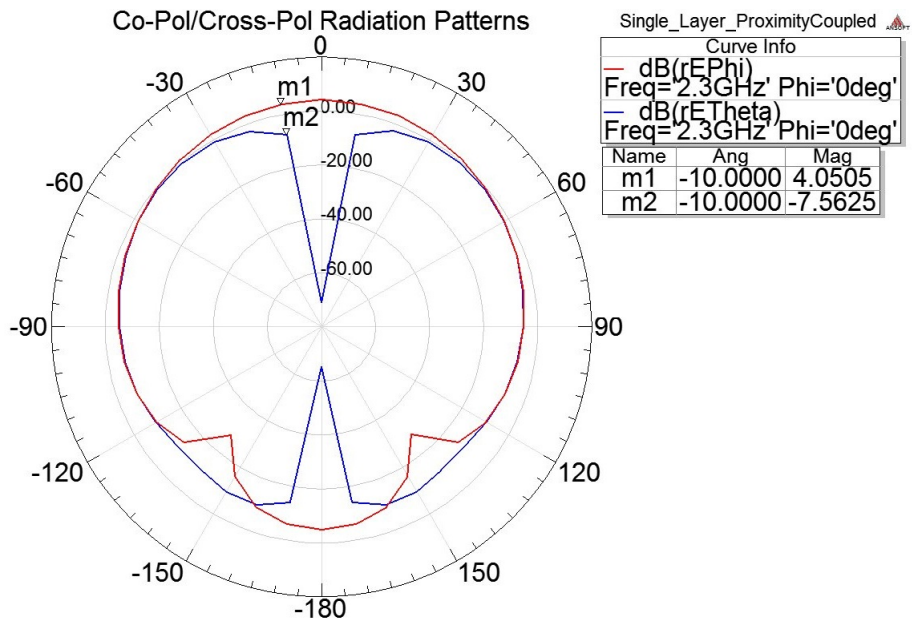
(b) Co-Pol/Cross-Pol for 2300 MHz at $\phi=0°$

Figure 2.3: Co-Polarization(Red) and Cross-Polarization(Blue) Radiation Patterns for 1500 MHz and 2300 MHz at $\phi=0°$

for higher frequencies, the radiation pattern in this plane is calculated for 2.8 GHz and plotted on the same graph. It can be observed that, even at 2.8 GHz, which is almost twice the starting frequency of the band, a null problem close to broadside direction does not occur. This may be due to the fields radiated by the feeding structure. Hence, even though the radiation from the feed structure

13
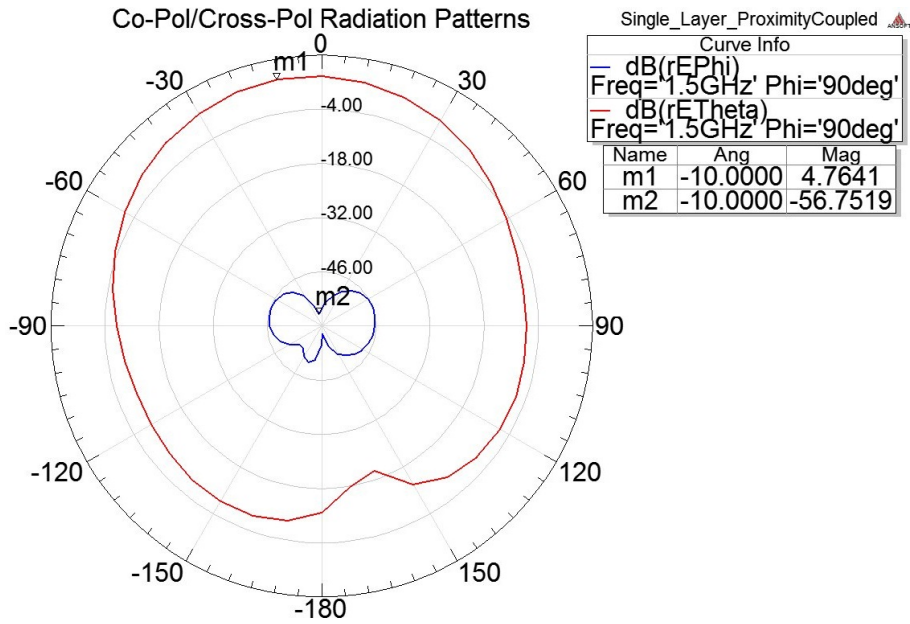
(a) Co-Pol/Cross-Pol for 1500 MHz at ϕ=90°
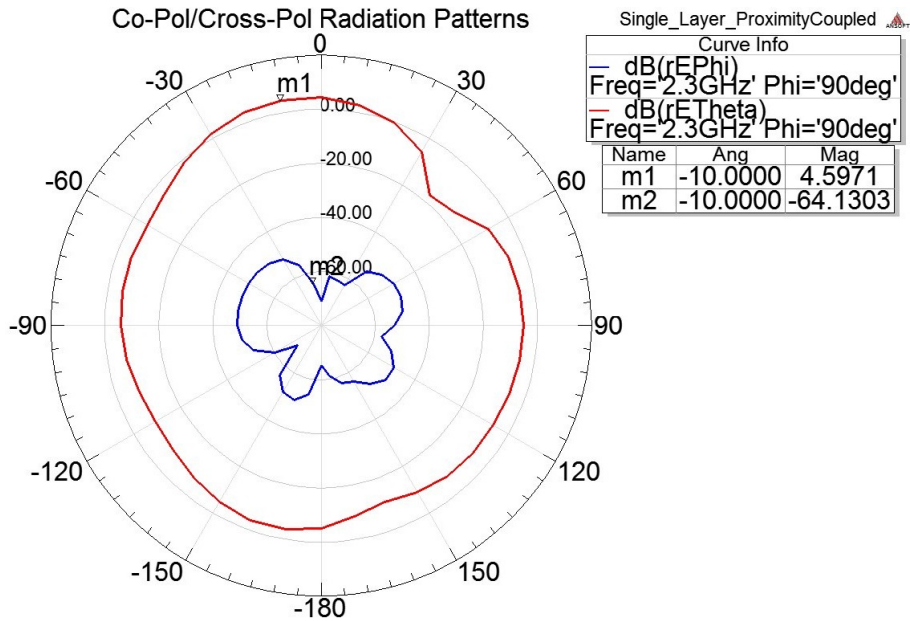
(b) Co-Pol/Cross-Pol for 2300 MHz at ϕ=90°

Figure 2.4: Co-Polarization(Red) and Cross-Polarization(Blue) Radiation Patterns for 1500 MHz and 2300 MHz at ϕ=90°

deteriorates the radiation performance at ϕ=0° plane by increasing the cross-polarization level, it improves the performance at ϕ=90° plane.

In addition to impedance bandwidth and radiation pattern analysis, surface currents for elevated strip and radiating patch are also analyzed. The current distributions at 1500 MHz and 2240 MHz are shown in Fig.2.7 and Fig.2.6,

14
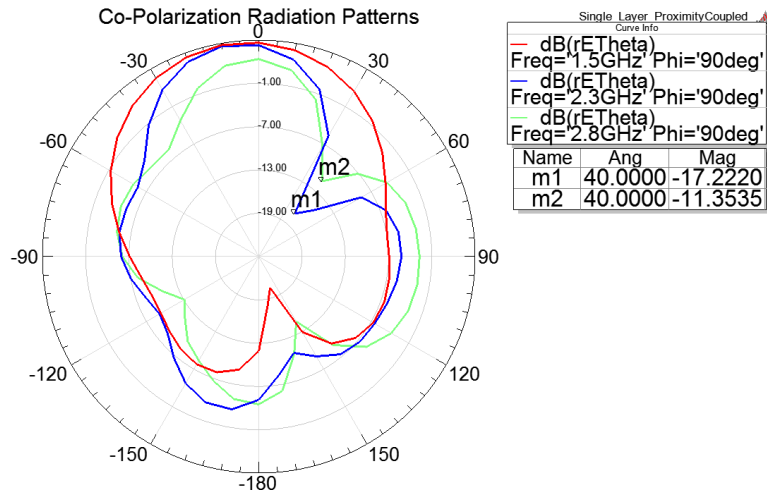
Figure 2.5: Co-Pol Radiation Patterns for 1500 MHz, 2300 MHz and 2800 MHz at ϕ=90°

respectively.

(a) J$_{surf,feed}$, Magnitude

(b) J$_{surf,feed}$, Vector

(c) J$_{surf,patch}$, Magnitude

(d) J$_{surf,patch}$, Vector
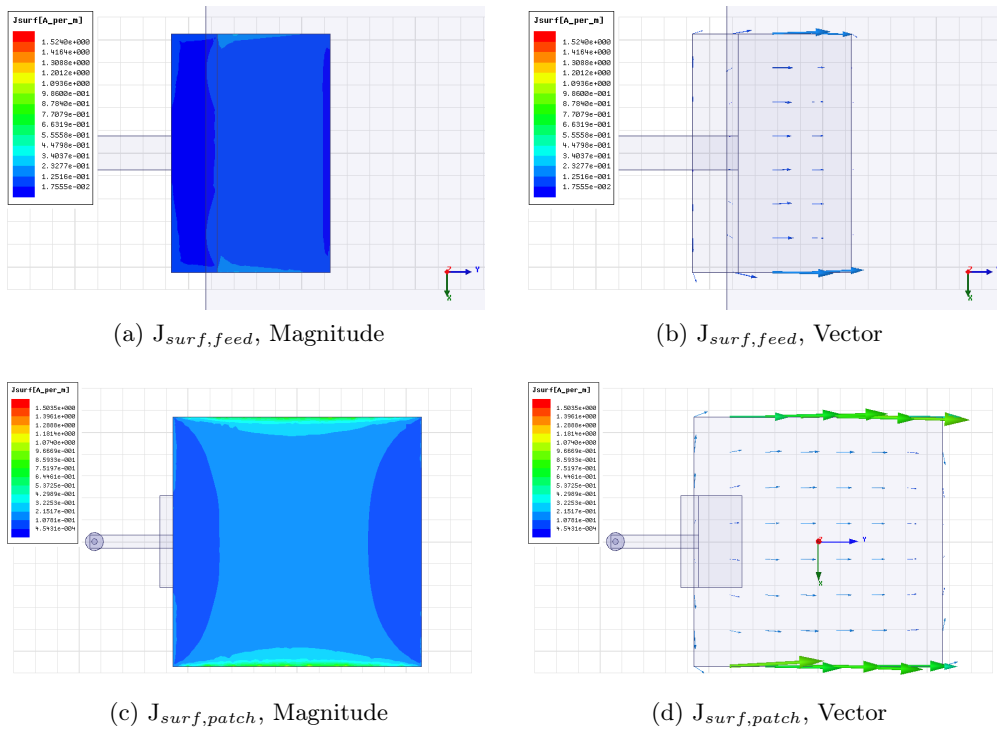
Figure 2.6: Surface Current Representations on Feed and Patch at 1500 MHz

As it can be seen from Fig.2.7 and 2.6, current flow is in the direction of feed and patch length respectively. However, at 2240 MHz, a current flow in the opposite direction on the back extension of the feed is observed. This is simply because of the T-Shaped structure of the feed patch and transition. The current coming

15

from the vertical strip of the feed distributes both to the left and to the right of the feed patch at the junction. As expected, distribution of J_{surf} is higher on radiating patch than the distribution of J_{surf} on feed at 1500 MHz, which is the resonant frequency of the radiating patch. Oppositely, distribution of J_{surf} is higher on feed than the distribution of J_{surf} on radiating patch at 2240 MHz, which is the resonant frequency of the feed. Besides, due to the radiation from feed structure, there occurs diffraction from the edge of the radiating patch, which yields surface current on the feed side edge of the patch, as shown in 2.7c.

(a) $J_{surf,feed}$, Magnitude

(b) $J_{surf,feed}$, Vector

(c) $J_{surf,patch}$, Magnitude

(d) $J_{surf,patch}$, Vector
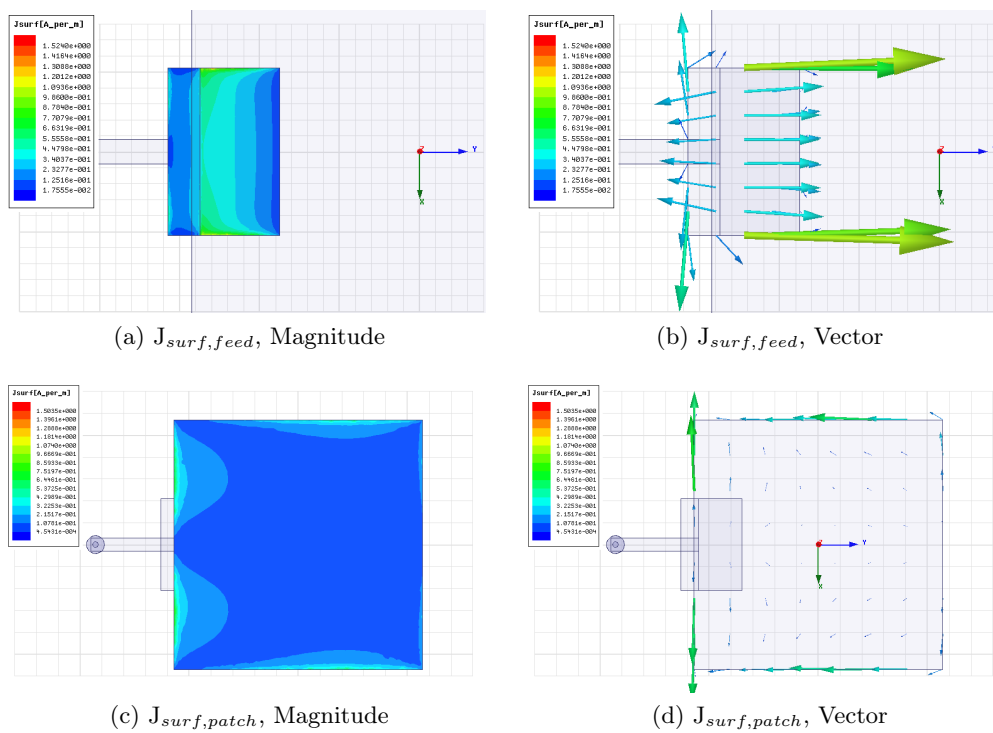
Figure 2.7: Surface Current Representations on Feed and Patch at 2240 MHz

Ideally microstrip patch antennas are polarized along the feed direction, which means surface currents are along feed direction. In our case it is in y-direction and because of that the structure is called y-polarized. However, due to the diffraction from the feed side edge, there occurs surface currents along the x-direction, which can be counted as one of the primary source of the cross-polarization. Hence the current distribution results also support the discussions about the radiation patterns.

2.1.1 Parameters and Parametric Analysis of a Single Rectangular Patch with a Single Electromagnetically Coupled Feed

The parameters used to analyze the given antenna, Fig. 2.1, are shown in Table 2.1. These parameters have an effect on the resonant frequency of feed and radiating patches, bandwidth and feed's electromagnetic coupling level. Parametric analysis is done by varying only one of the parameters within the range defined in Table 2.1's Range column. To be noted that, unless otherwise stated, optimum values are indicated with "0 mm" value of corresponding variables in legends.

Table2.1: Design Parameters for Single Rectangular Patch with a Single Electromagnetically Coupled Feed

Parameters	Description	Range	Nominal Value
L_{patch1}	Length of the Patch 1	[53mm, 61mm]	$57mm$
W_{patch1}	Width of the Patch 1	[53mm, 61mm]	$57mm$
h_{patch1}	Height of the Patch 1	[19mm, 25mm]	$21.4mm$
L_{feed1}	Length of the Feed 1	[12mm, 16mm]	$14mm$
W_{feed1}	Width of the Feed 1	[18.5mm, 24.5mm]	$21mm$
h_{feed1}	Height of the Feed 1	[14mm, 18mm]	$16mm$
y_{offset}	Offset intersection of feed patch and elevation patch	[0mm, 14mm]	$4mm$
x_{feed1}	Position relative to patch in x-direction	[-15mm, 15mm]	$0mm$
y_{feed1}	Position relative to patch in y-direction	[-4mm, 10mm]	$4mm$

2.1.1.1 Effects of Radiating Patch Length (L_{patch1}) Variations

As shown in Fig.2.2, maximum impedance bandwidth is achieved when $\text{L}_{patch1} = 57mm$ and the other design parameters stated in Table 2.1 are at nominal values. However, in order to understand the effects of patch length to input return loss, $\pm 4mm$ variation is applied. The corresponding results are shown in Fig.2.8.

As previously mentioned, in single elevated feed with a single patch design, there exists two resonant frequencies. One of them is radiating patch related (left most of the Fig. 2.8), the other is elevated feed patch related (right most of the Fig. 2.8).

According to the Fig. 2.8 there exists frequency shift to the left, i.e. as L_{patch1} in-
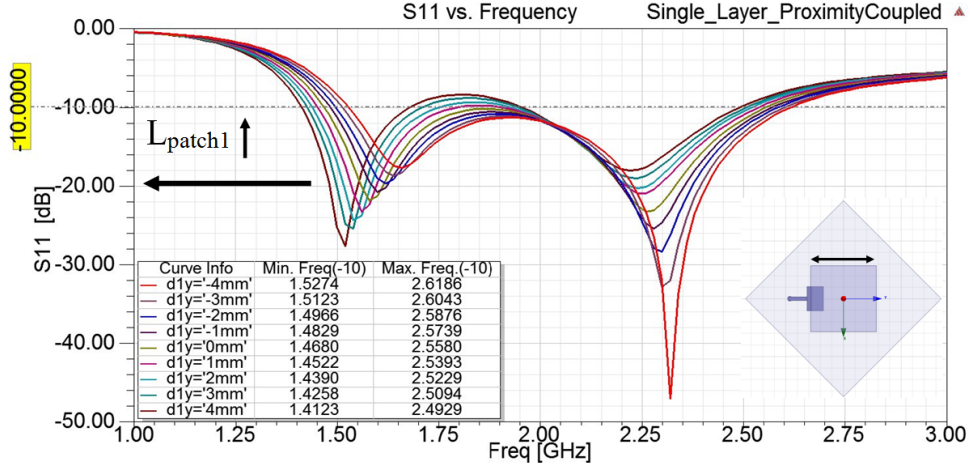
Figure 2.8: Effects of L_{patch1} Variations to Return Loss Characteristics of Single Rectangular Patch with a Single Electromagnetically Coupled Feed

creases, the resonant frequency of the radiating patch decreases. This frequency shift can easily be determined from Eq. 2.1 and Eq. 2.2.

Besides, L_{patch1} variations not only affect the radiating patch resonance, but also it shifts the resonant frequency of the feed to the left. Practically, if the feeding mechanism is something like a coaxial probe fed or edge fed type, the right most resonant frequency is not expected to be there. However, because of the proximity coupled feeding technique that is used in this study, as L_{patch1} increases, coupling between feed patch and radiating patch changes. And this yields a slight frequency shift to the left like radiating patch resonant frequency does.

In addition to these, as L_{patch1} increases, matching levels within the frequency band changes as well. As indicated in Fig. 2.8, while return loss characteristics around 1600 MHz is getting better with increasing L_{patch1}, it is getting worse around 2300 MHz. While trying to tune the antenna by adjusting L_{patch1} this behavior should be kept in mind.

2.1.1.2 Effects of Radiating Patch Width (W_{patch1}) Variations

As shown in Fig.2.2, maximum impedance bandwidth is achieved when W_{patch1} = 57 mm and the other design parameters stated in Table 2.1 are at nominal

18

values. However, in order to understand the effects of patch width to input return loss, ±4mm variation is applied. The corresponding results are shown in Fig.2.9.

It is well known that patch width variations do not affect the radiating patch resonant frequency. This fact can be observed from Fig.2.9 as well. The resonance around 1.6 GHz remains almost unchanged with respect to the variations in W_{patch1}. However, due to the coupling effect between feed structure and the radiating patch, W_{patch1} has an impact on return loss characteristics around 2300 MHz. As W_{patch1} increases, resonance around 2300 MHz slightly shifts left resulting in a slight decrease in overall impedance bandwidth. Consequently, it may be concluded that W_{patch1} is not an important parameter that affects the characteristics of the antenna. Therefore, it can be simply chosen to be equal to L_{patch1} for a dual polarization operation.
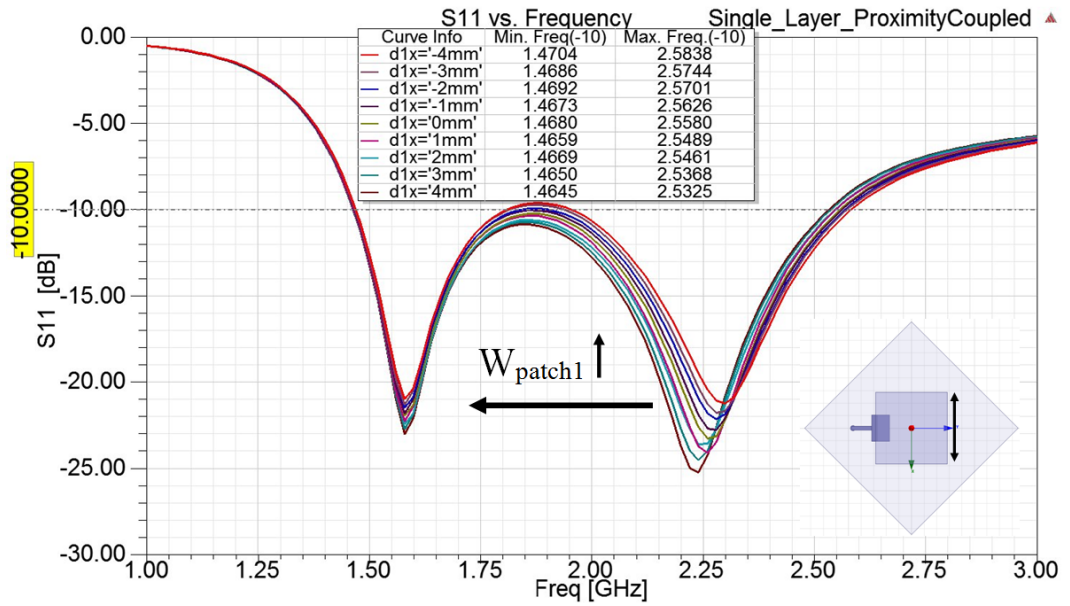
Figure 2.9: Effects of W_{patch1} Variations to Return Loss Characteristics of a Single Rectangular Patch with a Single Electromagnetically Coupled Feed

2.1.1.3 Effects of Radiating Patch Height (h_{patch1}) Variations

As shown in Fig.2.2, maximum impedance bandwidth is achieved when h_{patch1} = 21.4 mm and the other design parameters stated in Table 2.1 are at nominal values. However, in order to understand the effects of the height of the patch

from ground to input return loss, ±3mm variation is applied. The corresponding results are shown in Fig.2.10.
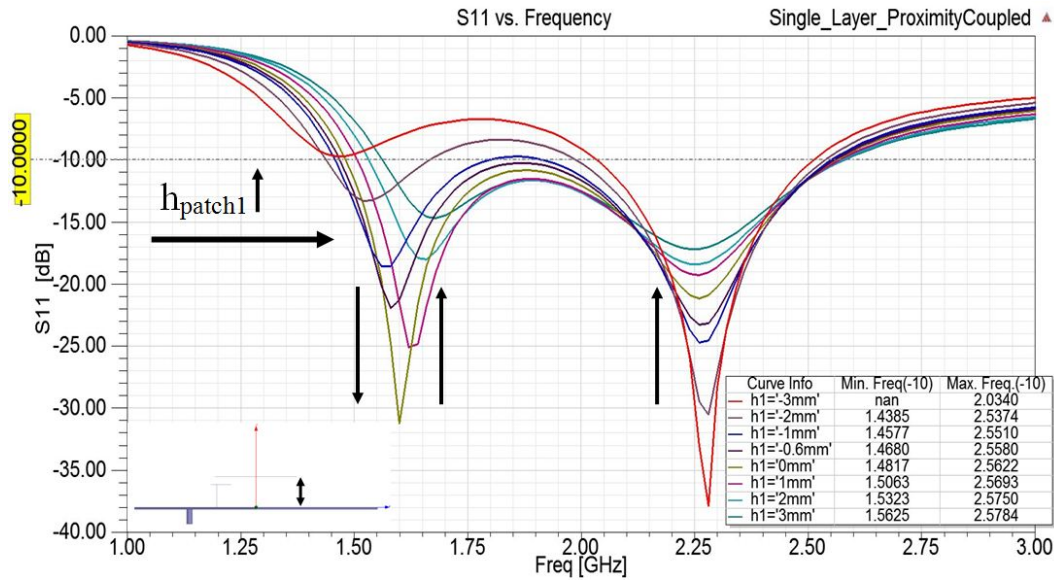
Figure 2.10: Effects of h_{patch1} Variations to Return Loss Characteristics of a Single Rectangular Patch with a Single Electromagnetically Coupled Feed

If we look at Fig. 2.10, there exists two major effects caused by h_{patch1} variation. The very first one is the matching level around the resonant frequency of the feeding structure (2300 MHz). As the height of the patch increases the matching level gets worse. Moreover, the behavior around the resonance frequency of the patch (1600 MHz) implies that the height of the patch changes the coupling level between the patch and the feed. Closely positioned patch results in over coupling and distant patch gives rise to under coupling. Therefore, the optimum height should be chosen accordingly.

2.1.1.4 Effects of Feed Patch Length(L_{feed1}) Variations

As shown in Fig.2.2, maximum impedance bandwidth is achieved when L_{feed1} = 14 mm and the other design parameters stated in Table 2.1 are at nominal values. However, in order to understand the effects of feed patch length on the input return loss, ±2mm variation is applied. The corresponding results are shown in Fig.2.11.

20
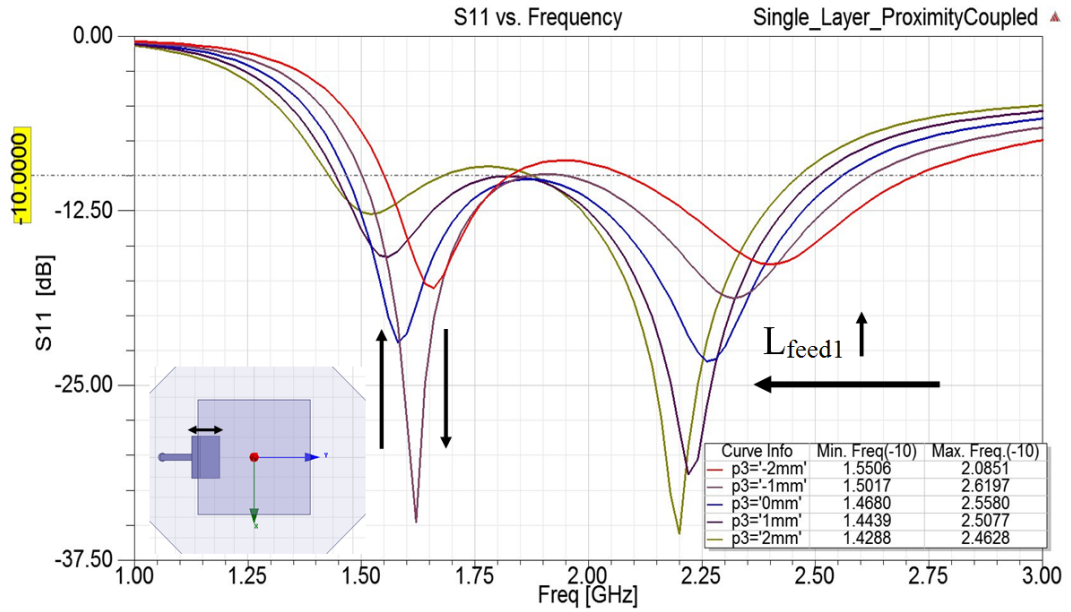
Figure 2.11: Effects of L_{feed1} Variations to Return Loss Characteristics of a Single Rectangular Patch with a Single Electromagnetically Coupled Feed

As expected, if the length of the feed increases, the corresponding resonant frequency around 2300 MHz decreases. Due to the coupling, this variation also moves the radiating patch resonant frequency to the lower frequencies. Besides, the length of the feed also affects the coupling level resulting in a variation in the return loss level of the first resonance.

2.1.1.5 Effects of Feed Patch Width (W_{feed1}) Variations

As shown in Fig.2.2, maximum impedance bandwidth is achieved when W_{feed1} = 21 mm and the other design parameters stated in Table 2.1 are at nominal values. However, in order to understand the effects of feed patch width to input return loss, ± 3mm variation is applied. The corresponding results are shown in Fig.2.12.

As we increase W_{feed1}, the resonance of the feed shifts slightly to lower frequencies and matching level at the resonance of the patch changes due to the change in the coupling level.
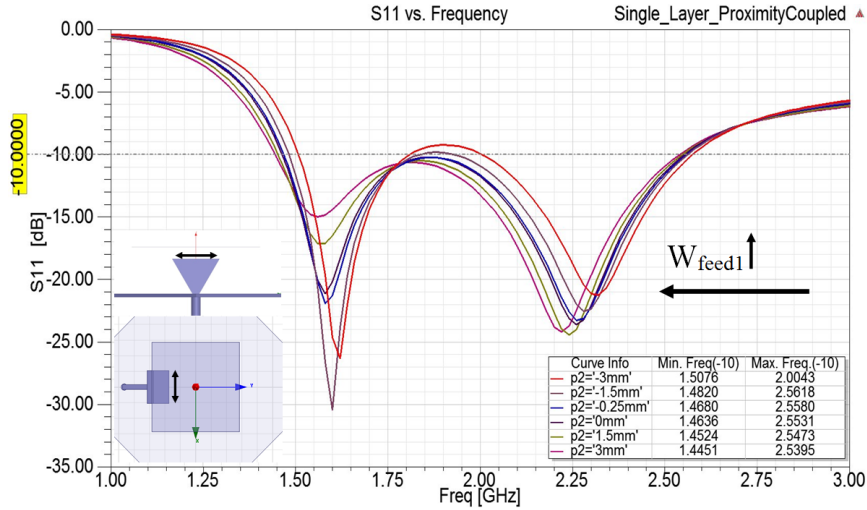
Figure 2.12: Effects of W_{feed1} Variations to Return Loss Characteristics of a Single Rectangular Patch with a Single Electromagnetically Coupled Feed

2.1.1.6 Effects of Feed Patch Height (h_{feed1}) Variations

As shown in Fig.2.2, maximum impedance bandwidth is achieved when h_{feed1} = 16 mm and the other design parameters stated in Table 2.1 are at nominal values. However, in order to understand the effects of patch height to input return loss, ±2mm variation is applied. The corresponding results are shown in Fig.2.13.
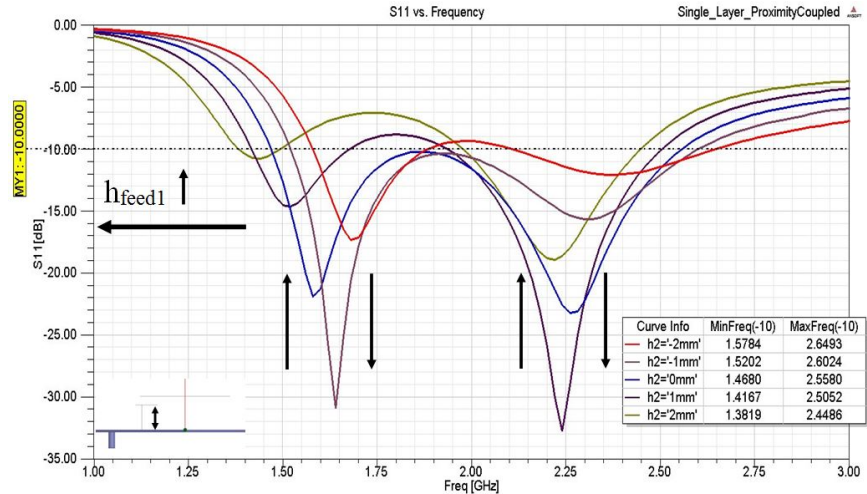
Figure 2.13: Effects of h_{feed1} Variations to Return Loss Characteristics of a Single Rectangular Patch with a Single Electromagnetically Coupled Feed

It is observed from Fig. 2.13 that, there exist two major effects caused by h_{feed1} variation. The very first one is the change in matching level of the resonance at

22

the feeding structure. There isn't a directly or inversely proportional variation with the change in the height of the feed. The matching level gets worse for very small height values because the tapered transition from the feed line to the feed patch becomes very abrupt. Similarly, the matching level also gets worse for very high thickness values due to the increase in the capacitive coupling as the feed patch gets close to the radiating patch. Therefore, the height should be optimized for the best matching. The second major effect is seen as a frequency shift on radiating patch resonant frequency. As h_{feed1} increases, there is a frequency shift to the left, which is the opposite of radiating patch height effect on radiating patch resonant frequency, as in Fig.2.10. This shift in the resonance frequency is due to the change in the coupling level between the patch and the feed. The change in the coupling level also effects the matching level at the resonance of the patch.

2.1.1.7   Effects of Feed Patch Offset (y_{offset}) Variations

As shown in Fig.2.2, maximum impedance bandwidth is achieved when $y_{offset} = 4$ mm and the other design parameters stated in Table 2.1 are at nominal values. However, in order to understand the effects of feed patch offset to input return loss, [0m, 14mm] variation is applied. The corresponding results are shown in Fig.2.14.

As y_{offset} increases, two resonance frequencies get closer to each other resulting in an improvement in the matching level for the frequencies between these two resonant frequencies. Therefore, this parameter can be optimized if the return loss is observed to be above -10 dB for the frequencies between these two resonant frequencies. It should be noted that the bandwidth becomes narrower as the two resonance frequencies get closer.
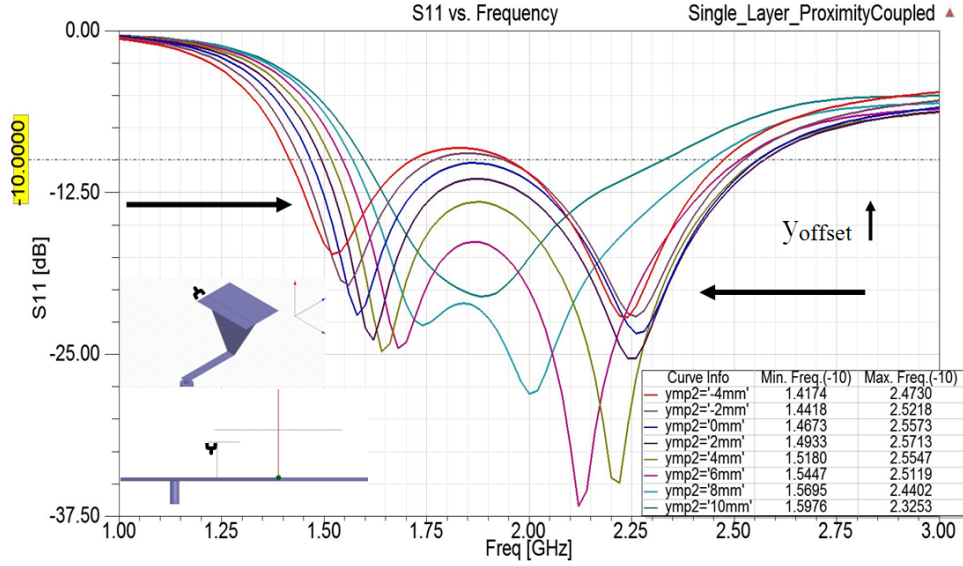
Figure 2.14: Effects of y_{offset} Variations to Return Loss Characteristics of a Single Rectangular Patch with a Single Electromagnetically Coupled Feed

2.1.1.8 Effects of Relative Feed Position Along x-axis(x_{feed1}) Variations

As shown in Fig.2.2, maximum impedance bandwidth is achieved when x_{feed1} = 0 mm and the other design parameters stated in Table 2.1 are at nominal values. However, in order to understand the effects of feed position along x-axis to input return loss, ±15mm variation is applied. The corresponding results are shown in Fig.2.15.

According to the simulation results shown in Fig. 2.15, as the distance from the center of the edge ($|x_{feed1}|$) increases, the resonant frequency around 2300 MHz is not affected, but the return loss level decreases, which means there occurs mismatch. Besides, as ($|x_{feed1}|$) increases, the feed comes close to the corners of the radiating patch. Because of this physical state, coupling between feed and radiating patch decreases. This situation yields a tiny effect on the resonant frequency of the radiating patch. From Fig. 2.15, as it is expected the response of the position variation along the patch width direction is symmetric relative to the center of the edge, so only 4 different plots are observed due to the symmetry.
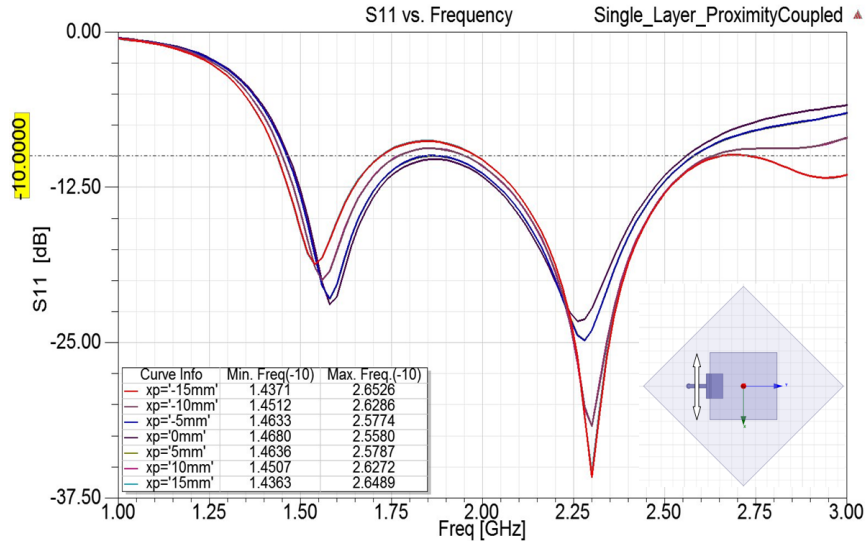
Figure 2.15: Effects of x_{feed1} Variations to Return Loss Characteristics of a Single Rectangular Patch with a Single Electromagnetically Coupled Feed

2.1.1.9 Effects of Relative Feed Position Along y-axis(y_{feed1}) Variations

As shown in Fig.2.2, maximum impedance bandwidth is achieved when $y_{feed1} = 4$ mm and the other design parameters stated in Table 2.1 are at nominal values. However, in order to understand the effects of feed position along y-axis to input return loss, [-4mm, 10mm] variation is applied. The corresponding results are shown in Fig.2.16.
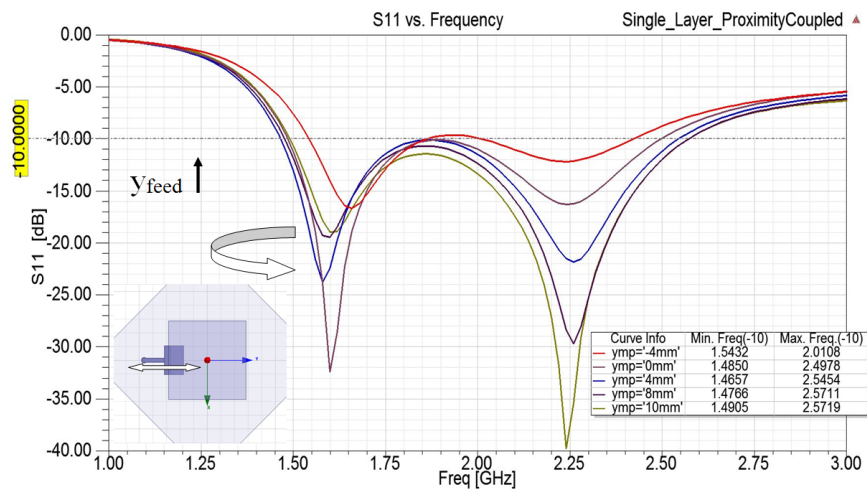
Figure 2.16: Effects of y_{feed1} Variations to Return Loss Characteristics of a Single Rectangular Patch with a Single Electromagnetically Coupled Feed

25

When y_{feed1} = -4mm, almost all of the feeding structure is out of extend of the patch. Therefore, the antenna is excited very weakly. On the other hand, the edge of the feeding patch coincides with the edge of the patch (i.e. feed is completely under the patch) when y_{feed1} = 8mm. As y_{feed1} increases the capacitive coupling between the patch and the feed structure changes and this affects the matching level at the resonance frequency of the feeding structure. Similarly, both the resonance frequency and the matching level of the patch also changes due to the variations in the coupling.

In the light of the observations made during the parametric analysis, a step-by-step guideline in order to start a similar design for a desired frequency band $[f_L, f_H]$ is proposed. According to the analysis done in previous sections(in our case $f_{r,patch}$=1500 MHz and $f_{r,feed}$=2300 MHz), following steps could be helpful for antenna engineers:

1. Specify ϵ_r, $f_{r,patch}$ (in MHz), h_{patch} (in cm) and h_{feed} (in cm)

   - ϵ_r=1 (due to air substrate),
   - $f_{r,patch}$= 1.1*f_L, $f_{r,feed}$ = 0.9*f_H,
   - Choose $h_{patch} \approx \dfrac{\lambda_{patch}}{10}$, $h_{feed} \approx \dfrac{\lambda_{feed}}{10}$.

2. Determine the effective relative permittivity(ϵ_{reff}) using Eq. 2.5

3. Determine the length of the patch using Eq.2.3

   - $L_{patch} + 2\Delta L = \dfrac{\lambda_{patch}}{2}$

4. Choose $\Delta L = h_{patch}$

5. Determine the length of the feed by assuming that the feed is monopole of length $\dfrac{\lambda}{4}$.

   - The total length of the feed assumed to be $L_{feed} + h_{feed}$ so;
     - $L_{feed} + h_{feed} = \dfrac{\lambda_{feed}}{4}$

6. Choose W_{patch} as L_{patch} in order to use this patch configuration for the dual polarized structure.

7. Initially calculate W_{feed} from the following ratio: $\frac{2}{3}$, which is determined from optimized structure dimensions in previous sections.

By the help of this step-by-step guide, the initial design parameters can easily be determined.

2.2 Simulations and Results for a Single Feed Single Patch Configuration for a Different Frequency Band

In order to show the results for application of guidelines between 3000 MHz - 5000 MHz frequency band, a single patch with a single elevated electromagnetically coupled feed configuration is designed and analyzed.

Design transformation of a single patch with a single elevated electromagnetically coupled feed configuration from 1.5 GHz - 2.5 GHz band to 3 GHz - 5 GHz band is performed. The steps used during this transformation is explained and corresponding results are presented and discussed.

According to the guideline and with some basic formulas, new design parameters for the new frequency band is obtained.
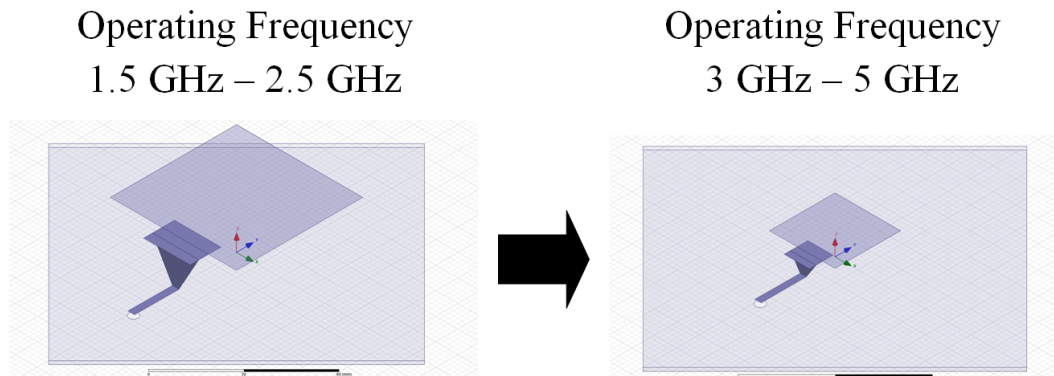
Figure 2.17: Frequency Band and Physical Dimension Transformations - Scaled View

As shown in Fig. 2.17, due to the operating frequency change to a higher frequency band, physical dimensions of the structure gets smaller. For the new frequency band, as the frequency is doubled compared to the previous design,

corresponding electrical length is halved. However, this scaling is used to determine the initial values of the parameters that are not discussed in proposed design guidelines.

$$\lambda = \frac{c}{f} \qquad (2.6)$$

According to the guideline presented in Section 2.1, following steps are followed:

1. Specify ϵ_r, f_L(in MHz), f_H(in MHz)

   - $\epsilon_r = 1$,
   - Set $f_L = 3000$ MHz and $f_H = 5000$ MHz
     - $f_{r,patch} = 1.1*f_L = 3300$ MHz,
     - $f_{r,feed} = 0.9*f_H = 4500$ MHz
   - Choose $h_{patch} \approx \frac{\lambda_{patch}}{10}$, $h_{feed} \approx \frac{\lambda_{feed}}{10}$.
     - $h_{patch} = 0.9$cm (9mm), $h_{feed} = 0.66$cm (6.6mm).

2. Determine the effective relative permittivity(ϵ_{reff}) using Eq. 2.5

   - Due to air filled substrate $\epsilon_{reff} = 1$

3. Determine length of the patch using Eq.2.3

   - $L_{patch} + 2\Delta L_{patch} = \frac{\lambda_{feed}}{2}$
     - $L_{patch} + 2\Delta L_{patch} = 45.45$ mm

4. Choose $\Delta L_{patch} = h_{patch} = 0.9$cm (9mm)

5. Determine length of the feed by

   - $L_{feed} + h_{feed} = \frac{\lambda_{feed}}{4}$
     - $L_{feed} + h_{feed} = 16.16$mm

6. Find L_{patch} and L_{feed}

   - Initial L_{patch} can be chosen as 27 mm from Step 3
   - Initial L_{feed} can be chosen as 10 mm from Step 5

28

7. Choose W_{patch} as L_{patch} in order to use this patch configuration for the dual polarized structure.

8. Initially calculate W_{feed} from the following ratio: $\frac{L_{feed}}{W_{feed}}$, therefore we know $L_{feed,new}$ from Step 4 and initial value can be found from $\frac{2}{3} = \frac{10mm}{W_{feed}}$ as 15 mm.

9. As we know L_{patch} from Step 6, y_{offset} value can also be calculated from the ratio $\dfrac{4}{10}$, which is determined from optimized design in previous sections.

   - From $\dfrac{4}{10} = \dfrac{y_{offset}}{10 - y_{offset}}$, y_{offset} can be calculated as 2.85 mm.

10. The distance between the intersection of transition and feed structure and projection of the radiating patch's edge to feed, as shown in Fig.2.18, can be found from the ratio of resonance frequencies of patch: the distance is inversely proportion with the ratio of resonance frequencies.
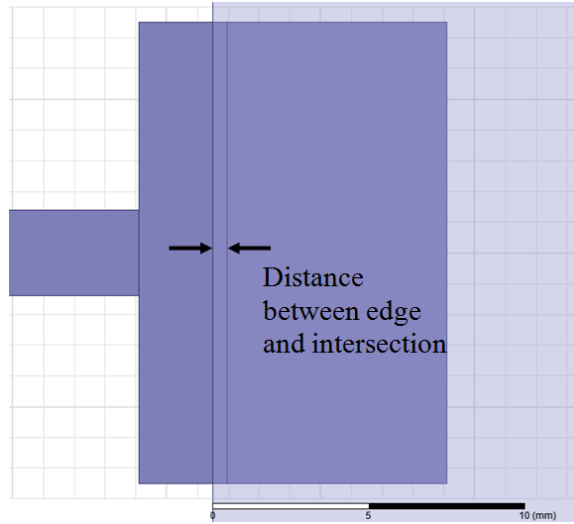
Figure 2.18

- $\dfrac{1.5GHz}{3.3GHz} = \dfrac{x}{1mm}$, where 1 mm is the optimized distance for 1.5 GHz.
- The distance can be found as 0.45 mm

The parameters determined from above steps are used to obtain initial design for a single patch single feed configuration operating between 3 GHz - 5 GHz frequency band. The corresponding simulation results for new design can be seen from Fig. 2.19. It can be easily examined that there are two resonant
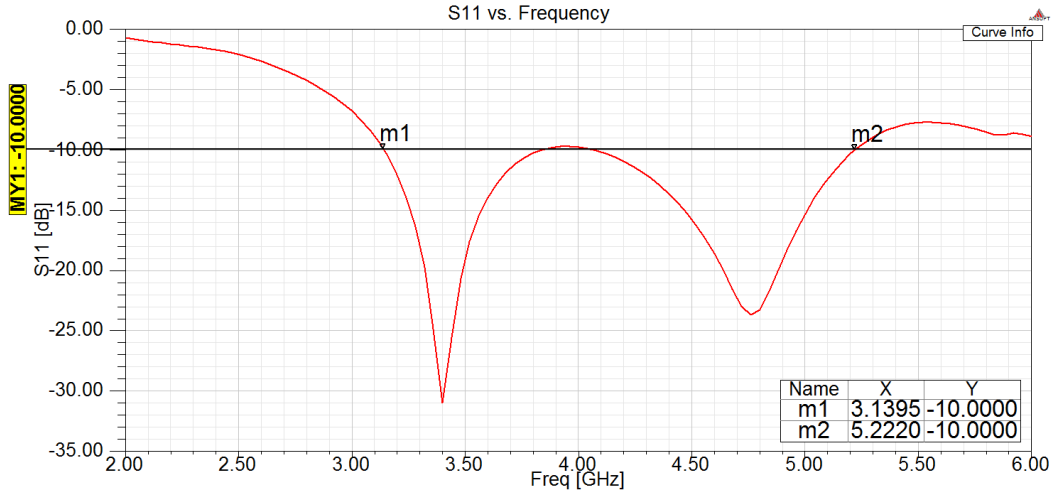
Figure 2.19: A Single Rectangular Patch with a Single Electromagnetically Coupled Feed S_{11} Characteristics for 3 GHz - 5 GHz Design

frequencies as previous design, which are around 3.4 GHz and 4.7 GHz related to radiating and feed patches, respectively. Obviously these parameters are for initial design, and they should be optimized in order to get widest impedance bandwidth within -10 dB return loss criteria.
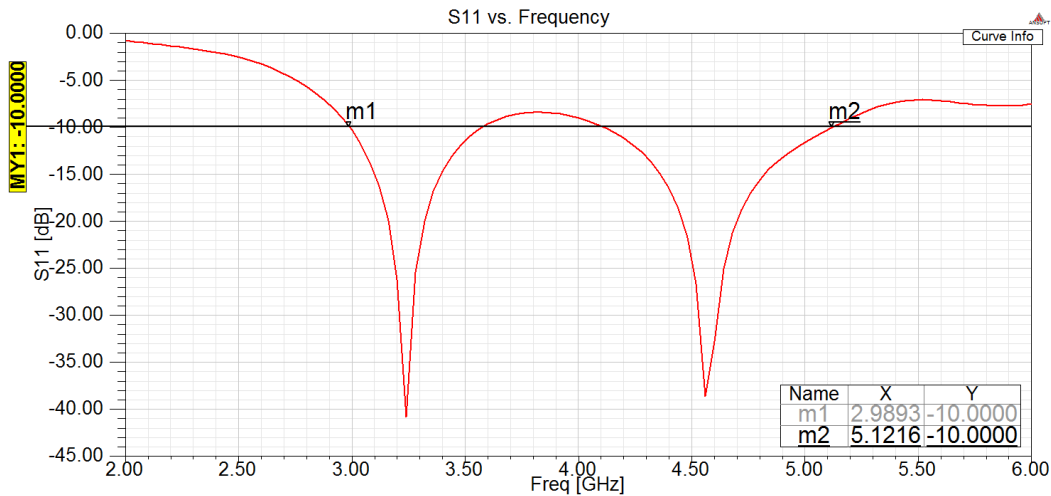
Figure 2.20: After Initial Design Optimization Results w.r.t W_{feed1}, L_{feed1} and L_{patch} Modifications

As proposed in Section 2, after getting initial design parameters and simulation results, there is applied some optimization to feed dimensions such as, L_{feed1}, W_{feed1} and L_{patch1}.

The optimization procedures are applied to W_{feed1}, L_{feed1} and L_{patch1}, because it is seen that there is a region that return loss is not below -10 dB threshold

30

value between the desired frequency band. In order to shift overall frequency characteristic to the left, W_{feed1} is chosen 1 mm smaller, L_{feed1} is chosen 0.5 mm bigger and L_{patch1} is chosen 2 mm bigger. L_{feed1} and L_{patch1} is chosen bigger, because due to the cavity model, as the length of the patch increases, the resonance frequency gets smaller. The corresponding acceptable return loss result is shown in Fig.2.20.

(a) 3D View
(b) Top View
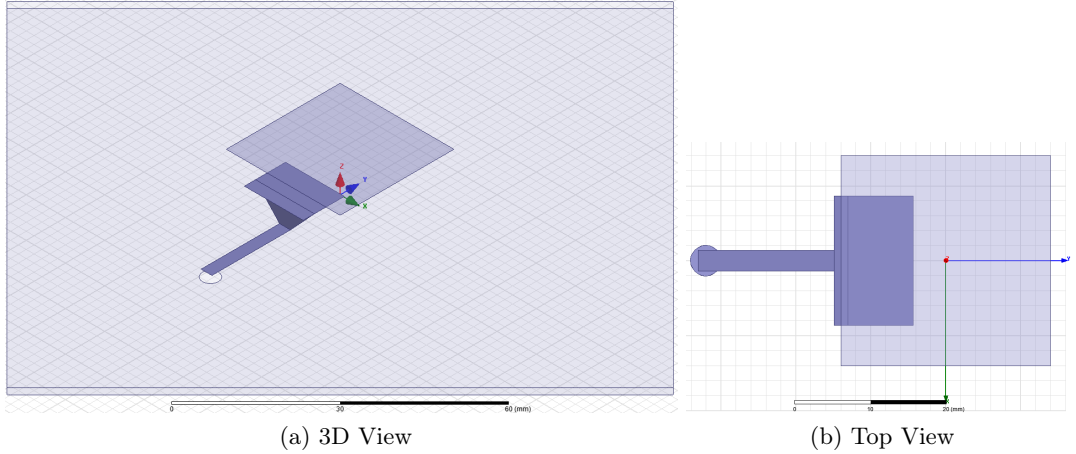
Figure 2.21: After Design Optimization - 3D and Top Views

Even the corresponding result is seen to be acceptable, if the Fig.2.21a and b is examined, design could not be accepted due to the W_{feed1} size, which limits the positioning of the second port for the dual polarization operation. In order to deal with this limitation, W_{feed1} should be reduced. However, if W_{feed1} gets smaller, although there occurs a slight shift in feed resonance, and no change in radiating patch resonance, as it can be seen from Fig.2.22c, return loss becomes larger than -10 dB for frequencies between 3.5 GHz and 4.2 GHz.

The return loss can be reduced below -10 dB level by making the resonant frequency of the patch and the feeding structure closer to each other. However, this will result in a narrower bandwidth. In order to achieve matching throughout the desired frequency band stacked patch configuration is tested.

In order to decrease the return loss value around 4 GHz, another parasitic patch with a resonance frequency around 4 GHz is put on top of the radiating patch. The resonance length of the patch is calculated by assuming that the radiating patch acts like the ground plane of this additional patch. This additional reso-

(a) 3D View

(b) Top View

(c) S_{11}
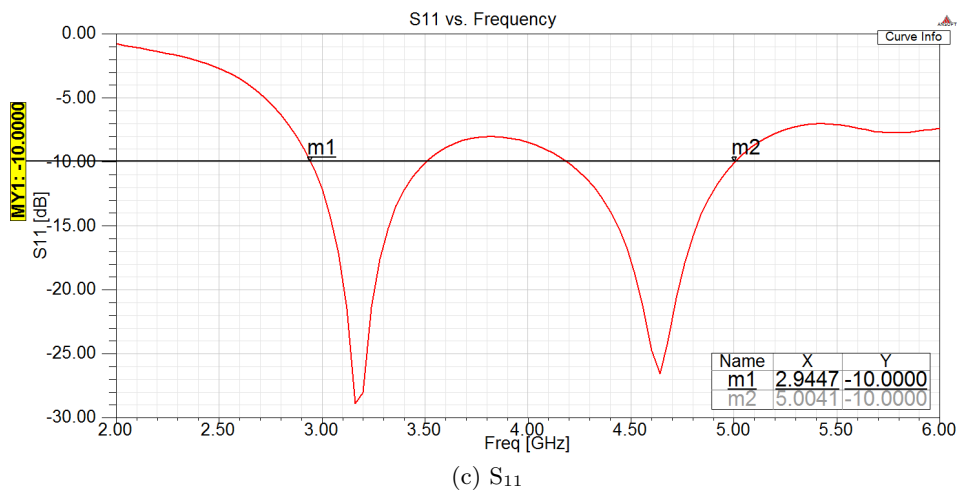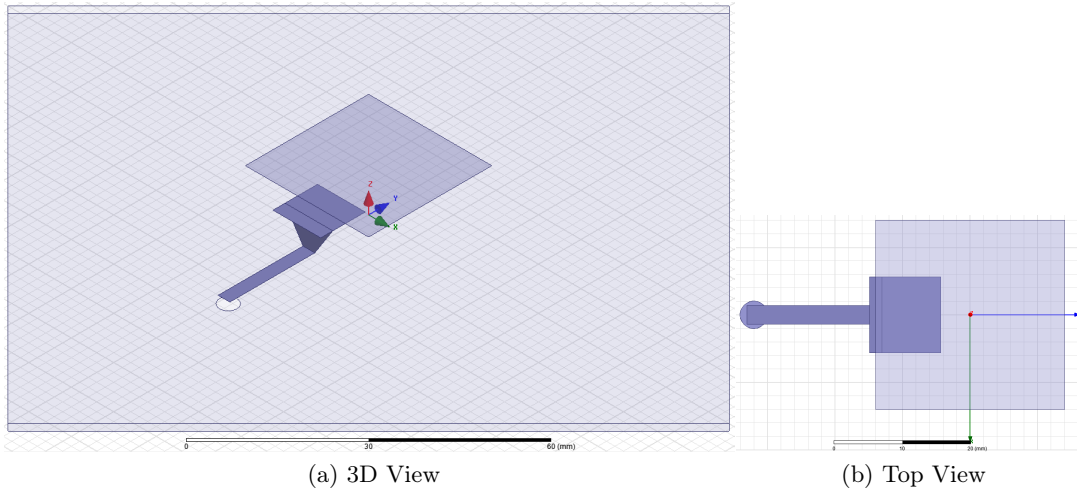
Figure 2.22: Return Loss After Size Limitation Optimization - Smaller W_{feed1} - 3D and Top Views

nant frequency makes our design acceptable within the required return loss value, and widens the impedance bandwidth as shown in Fig.2.23. From Fig.2.23, it can be seen that the overall design procedures are applied to have an antenna structure that operates at a different frequency band. For further improvement in return loss characteristic, additional modifications, i.e. iteratively tuning antenna parameters, could be applied as well.
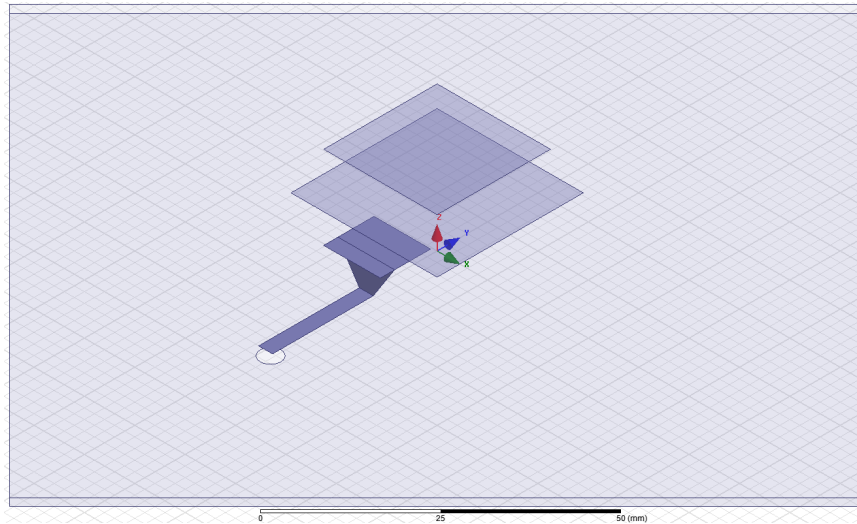
(a) 3D View
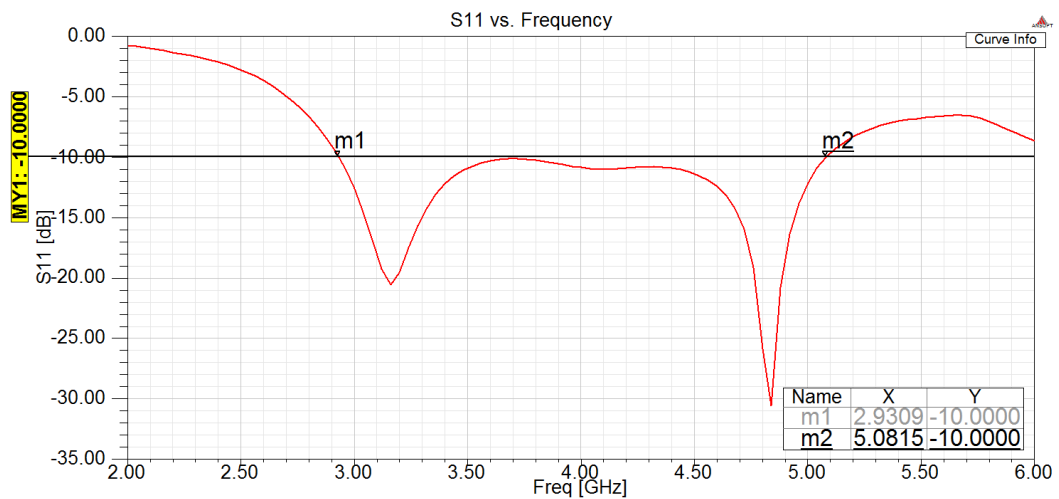
(b) S_{11}

Figure 2.23: Return Loss for Dual Layer Design- 3D View and S_{11}

2.3 Summary

In this chapter, an example of wideband electromagnetically excited patch antenna is analyzed and optimum design parameters are achieved with parametric analysis. The effects of physical parameters to impedance bandwidth are examined, co-polarization/cross-polarization analysis is done for optimum design and possible guidelines are reported.

Additionally, a demonstration of the guideline given in this chapter is performed. As given in guideline, two pre-calculated resonant frequencies are observed in return loss characteristic. Herein, it can be said that, given frequency bands

33

you can determine initial configuration parameters. However, in order to get the desired response for impedance bandwidth, optimization of the parameters needs to be done.

CHAPTER 3

ANALYSIS OF DUAL POLARIZED ANTENNA CONFIGURATIONS

In this chapter, the ability of designing dual polarized wideband antennas by using the antenna structure, which is studied in previous chapter, is demonstrated.

In the first part, an orthogonal feed is introduced. Because of the second port, the isolation between two ports is also examined. The effects of variations in the location of the feeds on the isolation are investigated.

In the second part, in order to improve the isolation between two orthogonal ports, an isolation wall is introduced and the effects of the isolation wall are analyzed.

In the last part two more patch elements are stacked above the radiating patch antenna to observe the performance of the stacked configuration.

3.1 Analysis and Design of a Single Rectangular Patch with Two Orthogonal Electromagnetically Coupled Feed

The structure of a single rectangular patch antenna with two identical orthogonal electromagnetically coupled feeds is given in Fig.3.1.

All the parameters of the antenna are kept fixed at the values presented in Table 2.1. Only position of the feeds $(x_{feed1}, y_{feed1}, x_{feed2}, y_{feed2})$ are optimized to improve the return loss and isolation characteristics of the dual polarized
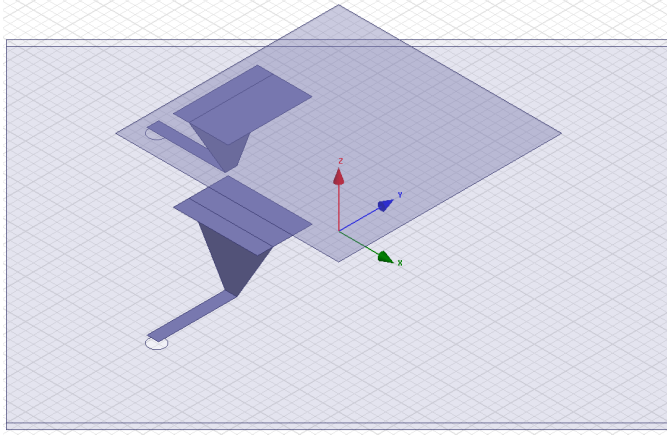
Figure 3.1: Structure of Single Rectangular Patch with Two Orthogonal Electromagnetically Coupled Feed

antenna. The optimized values are presented in Table 3.1 as nominal values. The return loss and the isolation performance of the antenna are presented in Fig 3.2 respectively.

Table3.1: Design Parameters for Single Rectangular Patch with Two Orthogonal Electromagnetically Coupled Feeds

Parameters	Description	Range	Nominal Value
x_{feed1}	Position relative to patch in x-direction of $feed_1$	[-5mm, 15mm]	$10mm$
y_{feed1}	Position relative to patch in y-direction of $feed_1$	[-4mm, 10mm]	$5mm$
x_{feed2}	Position relative to patch in x-direction of $feed_2$	[-4mm, 10mm]	$5mm$
y_{feed2}	Position relative to patch in y-direction of $feed_2$	[-5mm, 15mm]	$10mm$

As given in Fig.3.2, maximum impedance bandwidth and the best isolation level are achieved when x_{feed1} = 10 mm and y_{feed2} = 10 mm and the other design parameters stated in Table 2.1 and 3.1 are at nominal values. However, in order to understand the effects of feed positions along x-axis and y-axis for $feed_1$ and $feed_2$ respectively to input return loss and isolation of ports, these parameters are varied in [-4mm, 15mm] range. The corresponding results are shown in Fig.3.3.

According to the simulation results in Fig. 3.3a, as the orthogonal feeds run apart, red arrow, impedance bandwidth widens. In single feed configuration, analyzed in Chapter 2, the same variation does not have a significant effect on

36
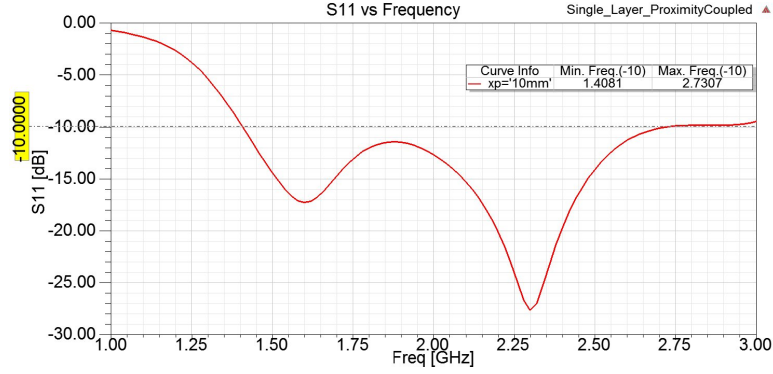
(a) S_{11}
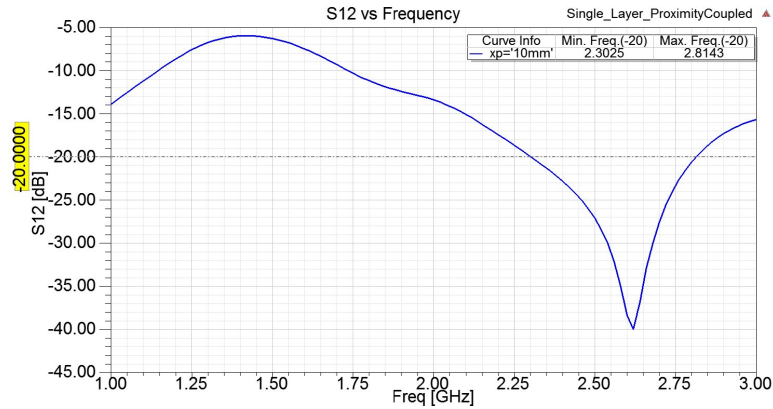
(b) S_{12}

Figure 3.2: Max Impedance Bandwidth and Best Isolation for Single Rectangular Patch with Two Orthogonal Electromagnetically Coupled Feeds

impedance bandwidth. However, in this case there occurs considerable bandwidth enhancement in S_{11}.

By introducing the second port, we have to take isolation between ports into account in order to get better results, including radiation efficiency, polarization and radiation pattern. Fig. 3.3b represents the isolation between two ports. Practically, if electromagnetically excited feeds are used for wide band applications, 20-25 dB isolation would be sufficient to get better polarization purity [11]. Due to the feeding technique that we use, if two orthogonal ports come close to each other, coupling between these ports would increase, which also means that the isolation level decreases, as shown in Fig. 3.3b with blue arrows. It is observed that by introducing the second port, S_{11} gets better and wider with respect to the single feed configuration, but isolation in that operating band is insufficient. Although the isolation gets better while the distance between two

ports increase, the frequency region that isolation is more effective is shifted to unwanted regions too. That's why the problem should be solved with some additional isolation techniques.
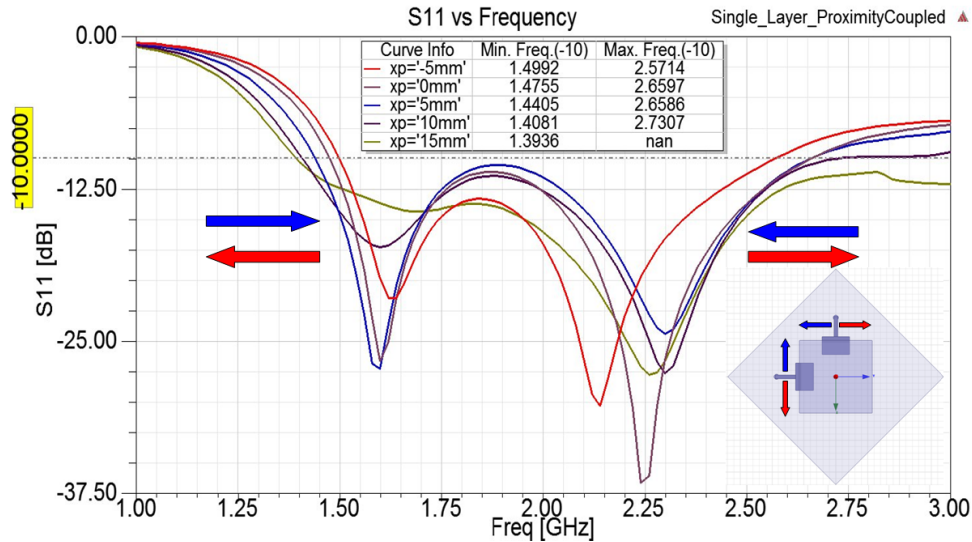
(a) S$_{11}$
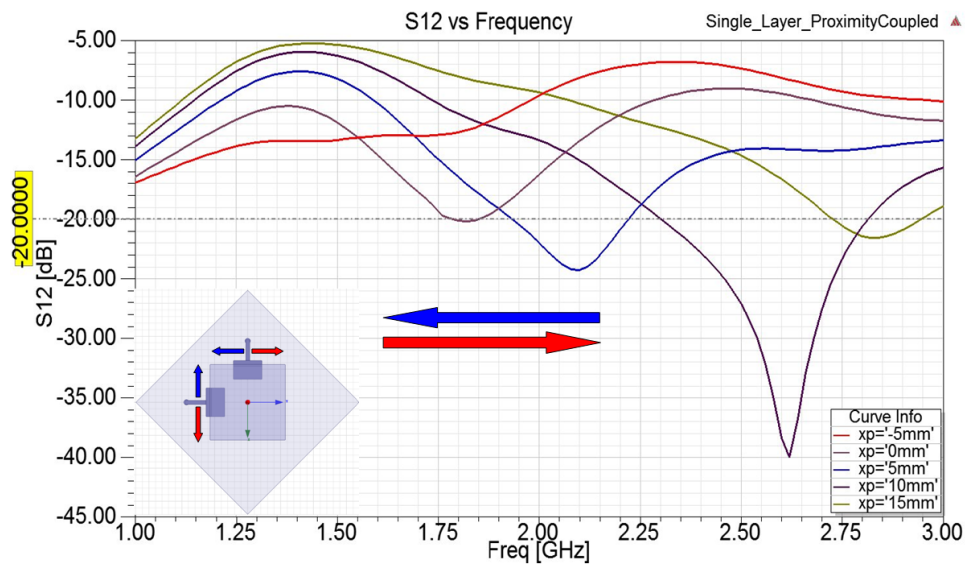
(b) S$_{12}$

Figure 3.3: Effects of x_{feed1} and y_{feed2} Variations to S$_{11}$ and S$_{12}$ Characteristics of Single Rectangular Patch with Two Orthogonal Electromagnetically Coupled Feeds

3.2 Analysis of a Single Rectangular Patch with Two Orthogonal Electromagnetically Coupled Feed and an Isolation Wall

In order to increase isolation level between two ports in the desired frequency band, an isolation wall is placed between two ports, as shown in Fig.3.4. This metallic blade is under the radiating patch and aligned with respect to the diagonal of the patch.
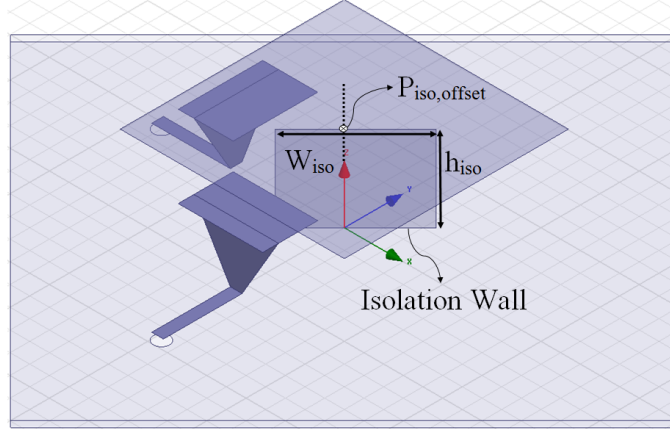
Figure 3.4: Structure of Single Rectangular Patch with Two Orthogonal Electromagnetically Coupled Feed and an Isolation Wall

Width(W_{iso}) and the diagonal position offset($P_{iso,offset}$) of the isolation wall are optimized and optimized values are given in Table 3.2. Height of the isolation wall (h_{iso}) is set as the height of the radiating patch (h_{patch1}). To observe the effects of these parameters parametric analysis is done by varying only one of the parameters within the range defined in Table 3.2's Range column.

Table3.2: Design Parameters for Single Rectangular Patch with Two Orthogonal Electromagnetically Coupled Feeds

Parameters	Description	Range	Nominal Value
W_{iso}	Width of the isolation wall	[25mm, 45mm]	$29mm$
$P_{iso,offset}$	Diagonal position offset w.r.t center of XY coordinate system	[-10mm, 10mm]	$-2mm$
h_{iso}	Height of the isolation wall	h_{patch1}	h_{patch1}

The optimum design is determined with the combination of widest impedance bandwidth at which the best isolation is achieved. The return loss and isolation performance of the antenna for the optimized values are shown in Fig. 3.5a and

b respectively. Fig. 3.5 shows that, the isolation wall has a significant effect on the isolation between two ports with respect to the configuration without that wall.

(a) S_{11}

(b) S_{12}
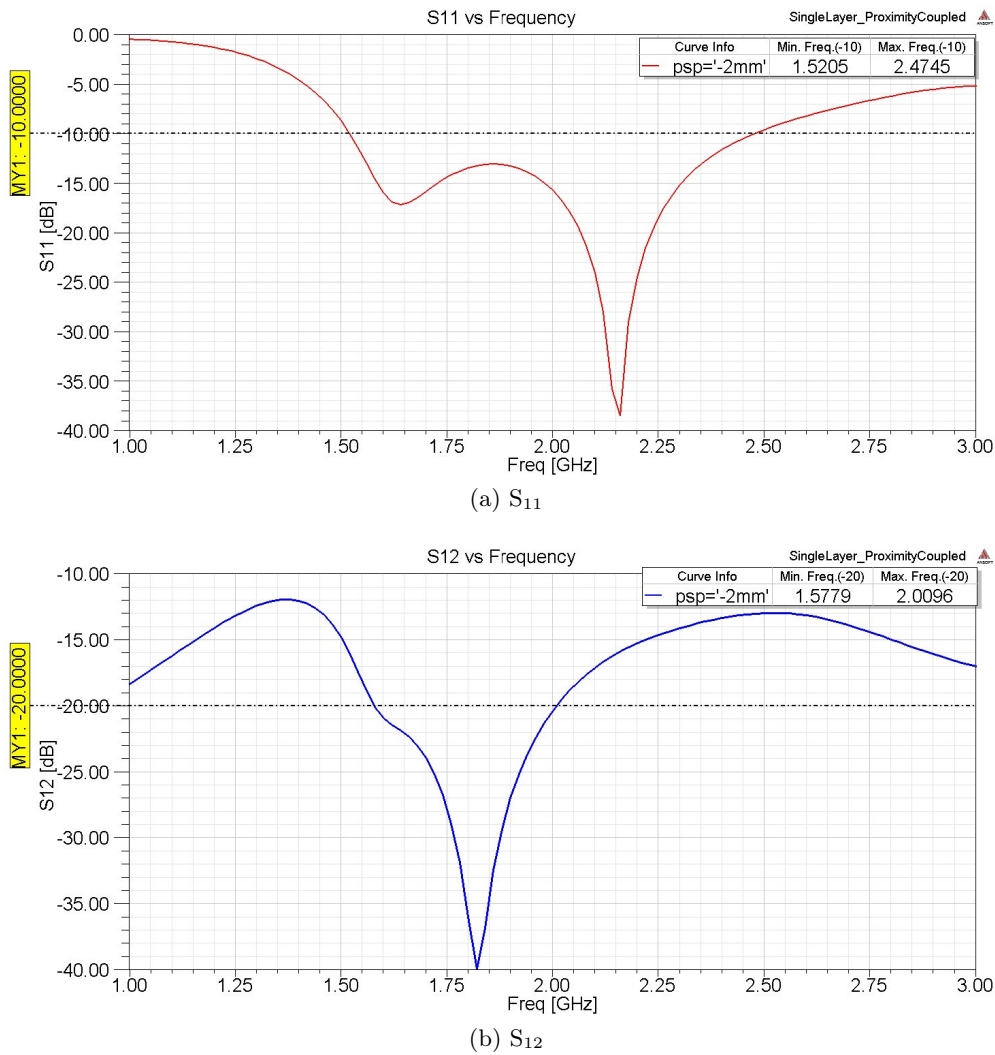
Figure 3.5: Max Impedance Bandwidth and The Best Isolation for Single Rectangular Patch with Two Orthogonal Electromagnetically Coupled Feeds and an Isolation Wall

3.2.1 Effects of Isolation Wall Width (W_{iso}) Variations

As given in Fig.3.5, maximum impedance bandwidth and the best isolation are achieved when $W_{iso} = 29$mm and the other design parameters stated in Table 2.1 and 3.2 are at nominal values. However, in order to understand the effects of diagonal isolation wall width to input return loss and isolation of ports, [0mm,

10mm] variation is applied. The corresponding results are shown in Fig.3.6.
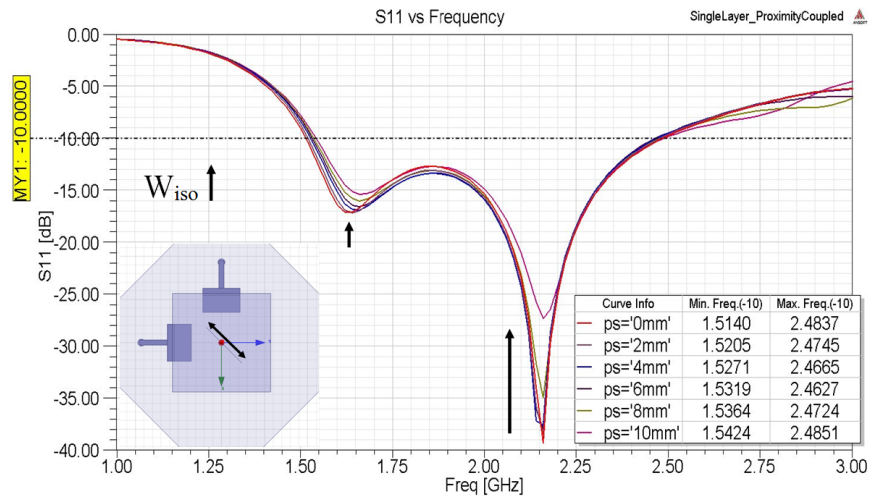
(a) S_{11}
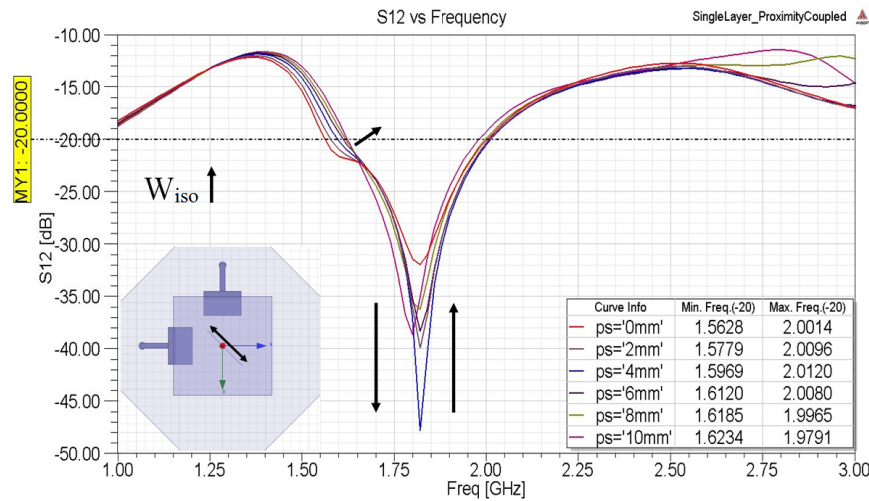
(b) S_{12}

Figure 3.6: Effects of W_{iso} Variations to S_{11} and S_{12} Characteristics of Single Rectangular Patch with Two Orthogonal Electromagnetically Coupled Feeds and an Isolation Wall

Variation on isolation wall width(W_{iso}) does not have a significant effect on both return loss and isolation. However, as W_{iso} increases, even if there is no frequency shift at resonant frequencies of both radiating patch and feed patch, there is still some considerable matching change at higher frequencies, Fig. 3.6a. This variation also affects the isolation strength around 1800 MHz. There occurs two different optimum points of where the isolation is the high but has a narrow band, and where the isolation is a little bit lower but has wider bandwidth.

According to the parametric analysis, optimum design parameters are reached, as stated in the beginning of Section 3.2.

3.2.2 Effects of Diagonal Position Offset ($P_{iso,offset}$) Variations

As given in Fig.3.5, maximum impedance bandwidth and the best isolation are achieved when $P_{iso,offset}$ = -2 mm and the other design parameters stated in Table 2.1 and 3.2 are at nominal values. However, in order to understand the effects of diagonal isolation wall position offset to input return loss and isolation of ports, ± 10mm variation is applied. The corresponding results are shown in Fig.3.7.

(a) S_{11}

(b) S_{12}
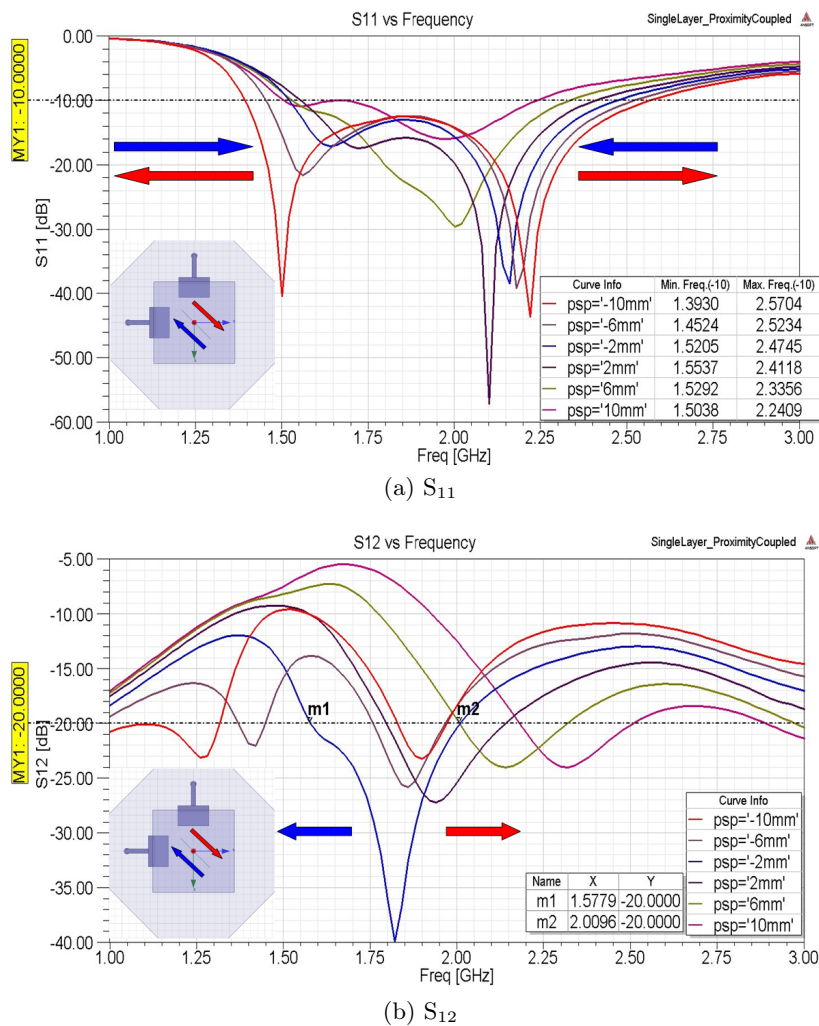
Figure 3.7: Effects of $P_{iso,offset}$ Variations to S_{11} and S_{12} Characteristics of Single Rectangular Patch with Two Orthogonal Electromagnetically Coupled Feeds and an Isolation Wall

42

According to the simulation results in Fig. 3.7a, as the isolation wall runs apart from the feeds, red arrow, there occurs considerable bandwidth enhancement in S_{11}. As it can be seen, the widest bandwidth is reached when the isolation wall is the farthest point from the feeds. However, at that point isolation level is neither in the considerable frequency region nor at the desired level. Therefore, the limiting factor for this structure is the best isolation point.

If we examine Fig. 3.7b, as $P_{iso,offset}$ varies the effective isolation region oscillates and at some points, lower frequencies have better isolation and at some points, higher frequencies have better isolation. However, between the nearest and farthest point there exists an optimum point that has the best isolation level between two ports. At the offset value where the best isolation level achieved the design has only 430 MHz S_{12} bandwidth(due to the -20 dB requirement) and 1.05 GHz S_{11} bandwidth(due to the -10 dB requirement). But still the limiting factor for the design is isolation level.

3.3 Stacked Antenna Configuration

In this section, the stacked configurations shown in Fig.3.8 are studied in terms of their input return loss, isolation and radiation characteristics.

<div align="center">(a) Single Layer   (b) Dual Layer   (c) Triple Layer</div>
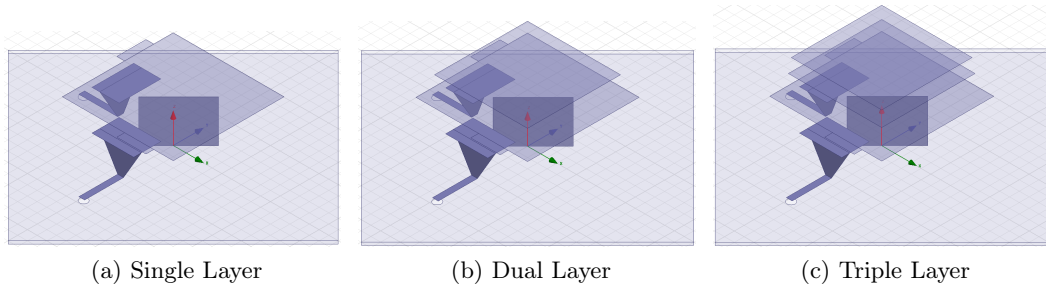
Figure 3.8: 3D Views of Dual Polarized Single, Dual and Triple Layered Patch Antenna Configurations

The corresponding design parameters for related analysis are acquired from a previously designed and measured stacked patch antenna configuration. The corresponding input return loss and isolation graphs are shown in Fig.3.9.

According to the simulation results shown in Fig.3.9a and b, it is observed that

(a) S_{11}

(b) S_{12}
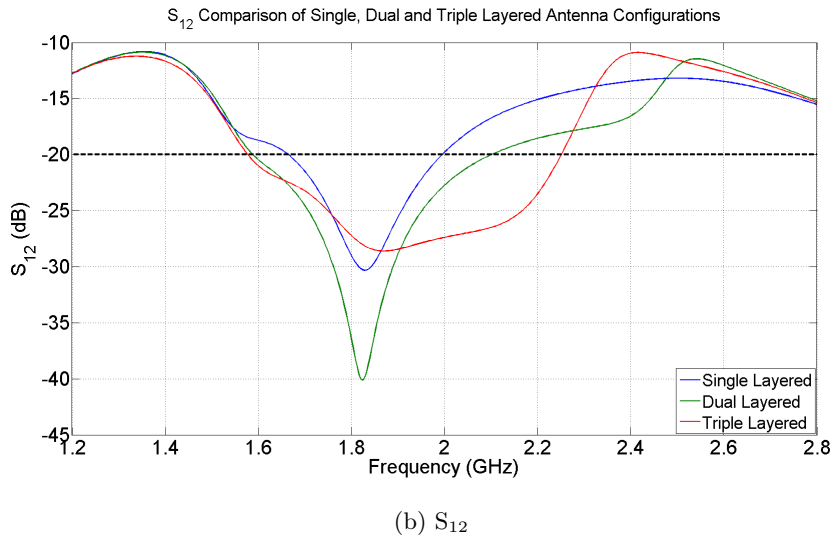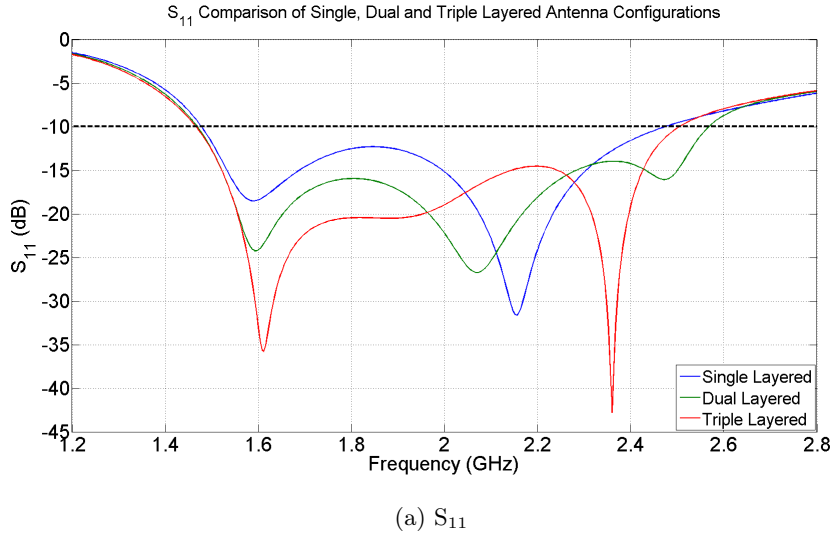
Figure 3.9: Effects of Stacks to S_{11} and S_{12} Characteristics

even though the overall characteristics of S_{11} has changed as the number of stacks increases, impedance bandwidth of S_{11} for a given threshold value, -10 dB, is not affected so much. On the other hand, there is a considerable effect of stack number on the isolation level, S_{12}, between two orthogonal ports. As the number of stacks increases, as patches for higher resonant frequencies are introduced, the isolation between ports gets better over the frequency band, and thus the overall impedance bandwidth of the structure gets better as well. This improvement could be because of the field cancellations due to the opposite phase components of the related fields or physical blocking effect of second and third patches with the air substrate.

In this part, the effects of number of stacked elements on the radiation characteristics are examined and the corresponding radiation patterns are shown in Fig.3.10.
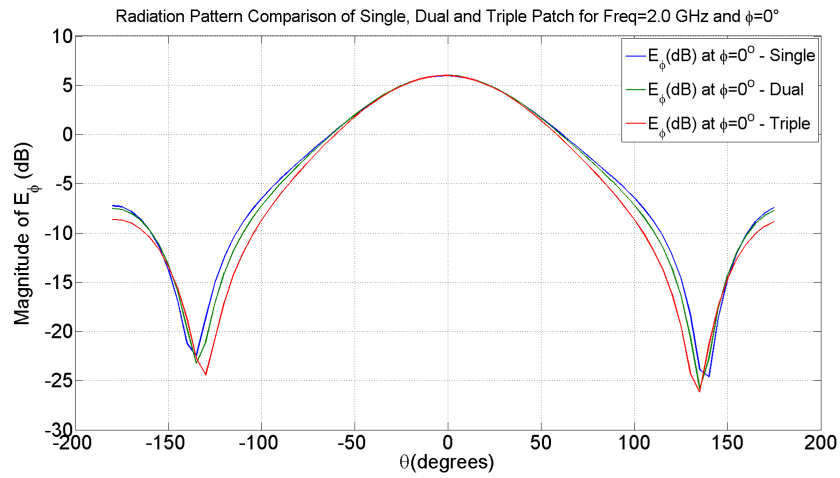
(a) For 2000 MHz
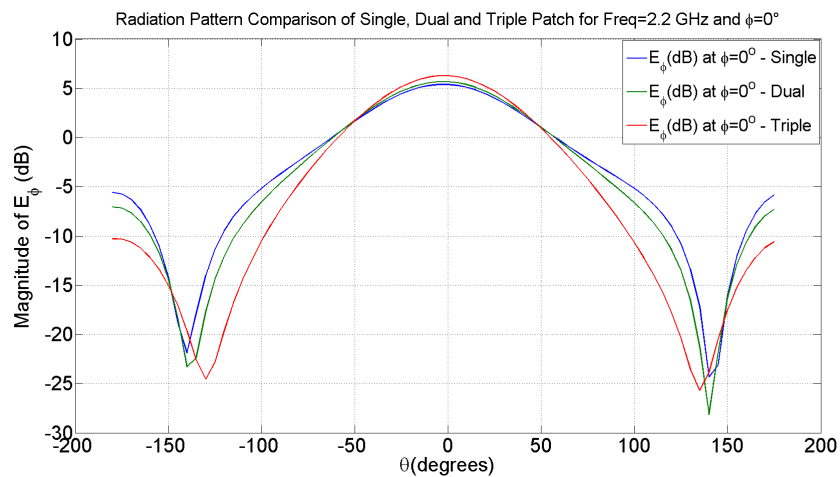
(b) For 2200MHz

Figure 3.10: Effects of Stacks to Radiation Pattern Characteristics

According to the simulation results shown in Fig.3.10, it can be said that apart from a slight decrease on the beamwidth of the antenna, no significant effect of additional parasitic patches are observed on the radiation characteristics of the antenna.

CHAPTER 4

COMPARISON OF SIMULATIONS AND MEASUREMENTS OF TWO-ELEMENT ARRAY

In this chapter, a two element array, Fig.4.1, formed by using dual polarized stacked patch elements are measured and the measurement and simulation results are compared.
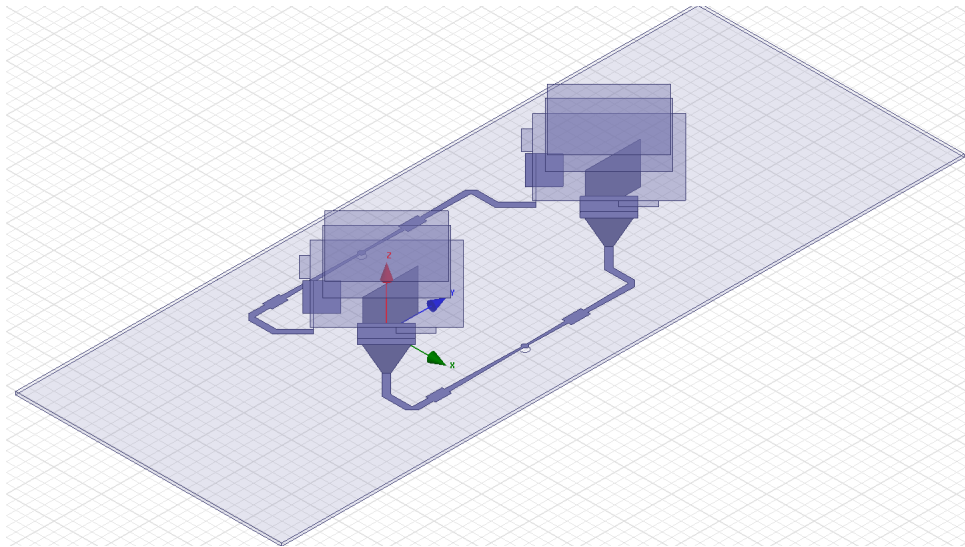
Figure 4.1: 3D View of Array Structure

All the parameters of the two element array are shown in Fig.4.2, 4.3, 4.4. The matching stubs on the feed lines are inserted to tune the frequency band of the manufactured array to the desired band.

Simulation and measurement results for the return loss characteristic and isolation are compared in Fig. 4.5. In both Fig. 4.5a and 4.5b, solid blue lines correspond to the measurement data of the fabricated array structure. The leg-
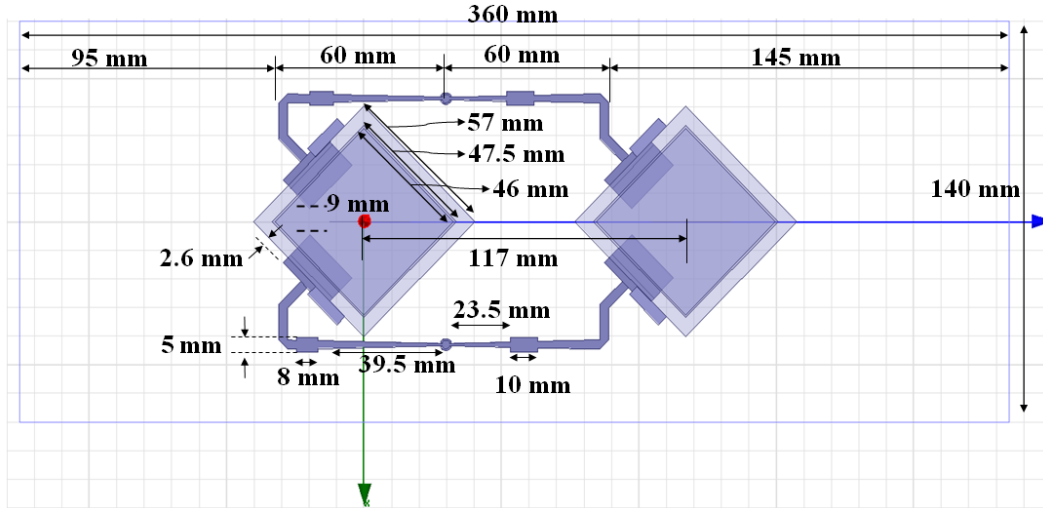
Figure 4.2: Two-Element Array Design Parameters of Dual Polarized Stacked Patch Antenna -1

end tag 'Simulation - Single' represent the simulation data for a single element. The last tag 'Simulation - Array' stands for the simulation data obtained for the array structure.

As shown in Fig. 4.5a, in lower frequencies, overall characteristic of the return loss for array structure is very similar in simulation and measurement wise. A slight resonance is seen in simulation data around 2050 MHz like in measurement data. However, as frequency gets higher, simulation and measurement data takes apart from each other. If we look at the 'S$_{12}$ - Simulation - Array' in Fig. 4.5b, measurement data is something like a squeezed version of simulation data, except the deep isolation around 1850 MHz. This may be because of an out of phase cancellation around that frequency in fabricated structure. Besides, it is observed that the 'S$_{11}$Simulation - Single' has exactly same behavior with the 'S$_{11}$ - Measurement' at higher frequencies. This behavior is valid for 'S$_{12}$ - Simulation - Single' as well. This differentiation may occur because of the small dimension errors or material that is used for simulation and fabrication.

Radiation pattern measurements are carried out in Aselsan Inc. Antenna Labs with Satimo Starlab Near Field Measurement System.

As shown in Fig.4.6a and Fig.4.6b, the measurement setup consists of a near
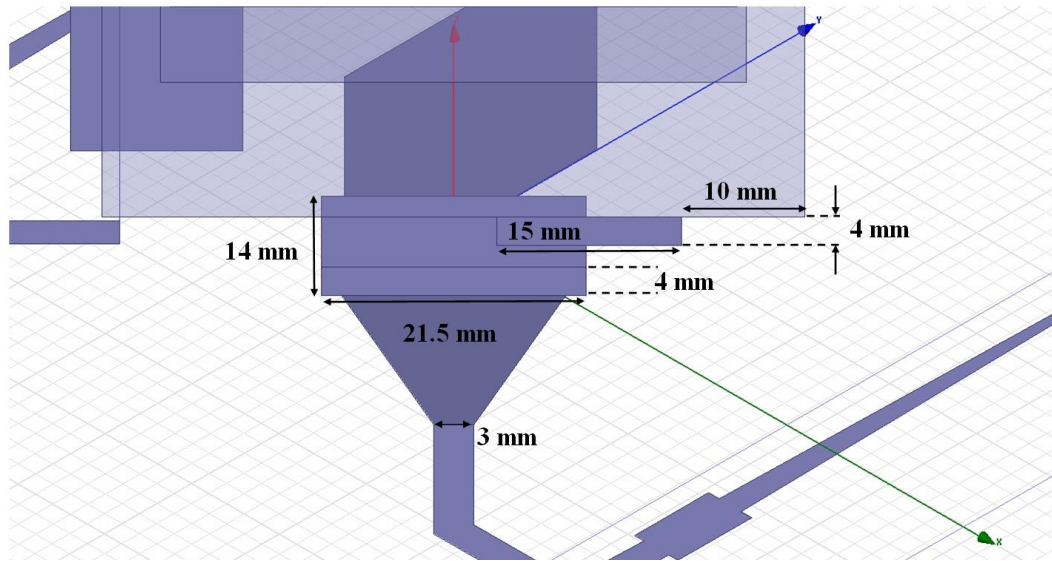
Figure 4.3: Two-Element Array Design Parameters of Dual Polarized Stacked Patch Antenna -2
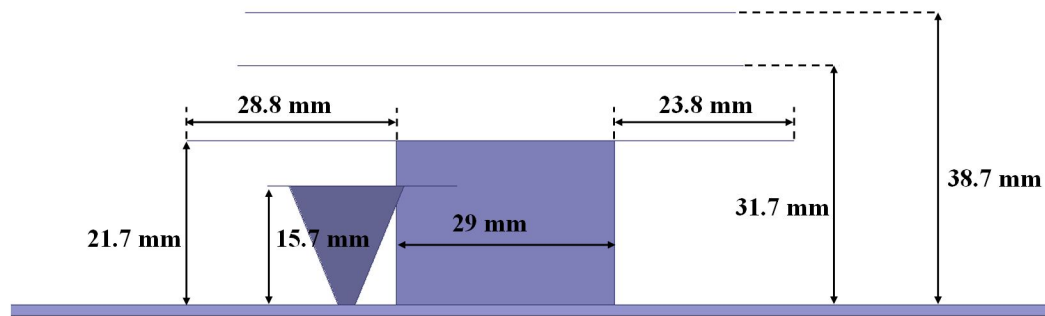
Figure 4.4: Two-Element Array Design Parameters of Dual Polarized Stacked Patch Antenna -3

field scanner and a remote control system. The near field scanner has the ability of measuring both vertical and horizontal polarizations with a '+' sign shaped probe.
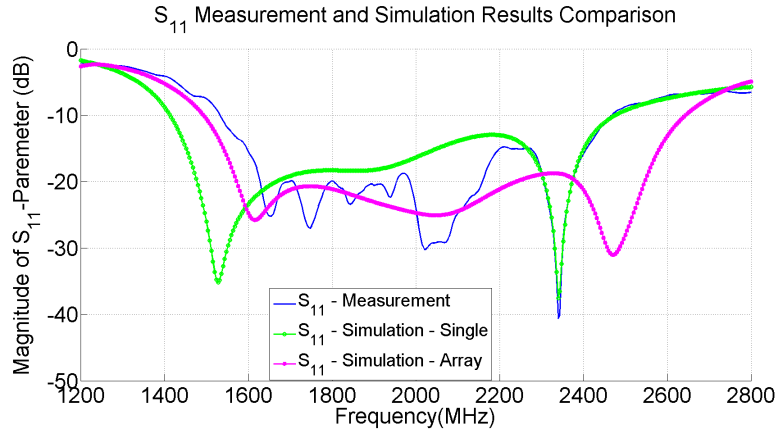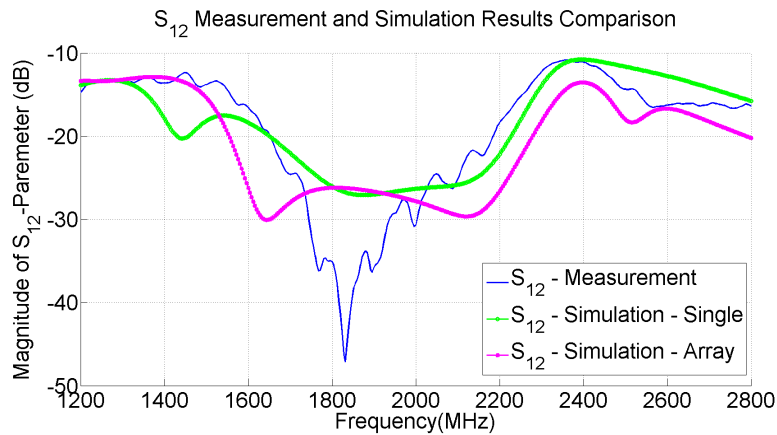
Figure 4.5: S_{11} and S_{12} Comparison of Measurement and Simulation Data for Dual Polarized Electromagnetically Excited Stacked Patch Two-Element Array

Measurement is carried out with the following properties:

- Frequency Range : 1 GHz - 3 GHz

- Step size : 5 MHz (401 points)

- Spatial Resolution : 11.25° grid size

- Antenna Diameter : 0.4 m

- Second port, corresponding to the other polarization, is terminated with 50Ω

After the setup activity is completed, the measurement is started. To be noted, according to the alignment of the antenna, the projection of the topmost scanner

50
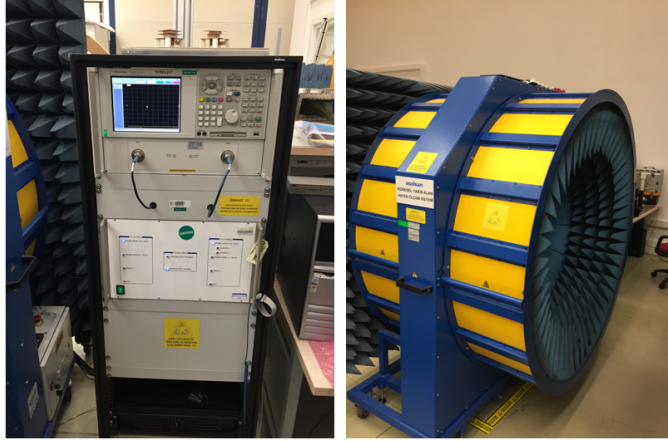
(a) Measurement Setup - 1
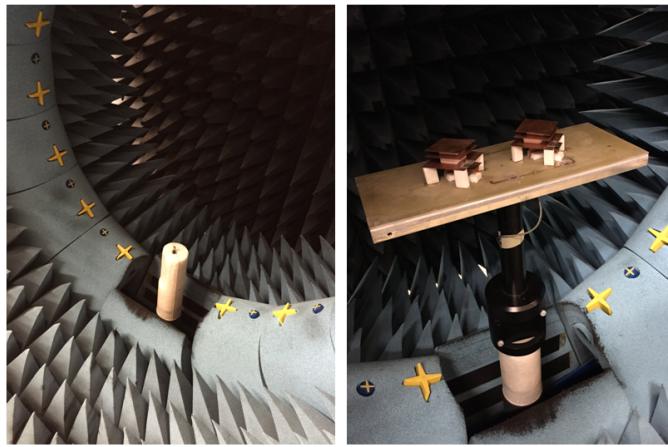
(b) Measurement Setup - 2

Figure 4.6: Measurement Setup for Dual Polarized Electromagnetically Excited Stacked Patch Two-Element Array

probe is seen for in Fig.4.7 for $\phi=0°$ and $\phi=+45°$ planes. When the receiver probe on the measurement system is aligned with the polarization of the antenna, as in Fig. 4.7b, we can talk about co-polarized and cross-polarized components. This alignment enables us to examine co-polarization at $\phi=45°$ with ϕ component and at $\phi=135°$ with θ component. Cross-polarization analysis can also be performed with the other way around with respect to co-polarization, such as at $\phi=45°$ with θ and at $\phi=135°$ with ϕ.

After measurement is completed, the overall measured data is filtered out to analyze E_{total}, E_{ϕ}, E_{θ}. First of all, E_{total} at $\phi=0°$ and $\phi=90°$ planes are obtained from the measured data, and presented in Fig.4.8. Since the polarizations of the antenna and receiver probe are not aligned in these planes, only E_{total} is
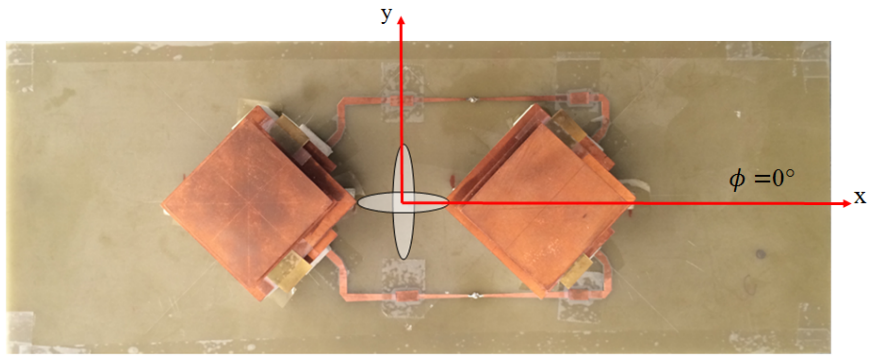
(a) at $\phi=0°$
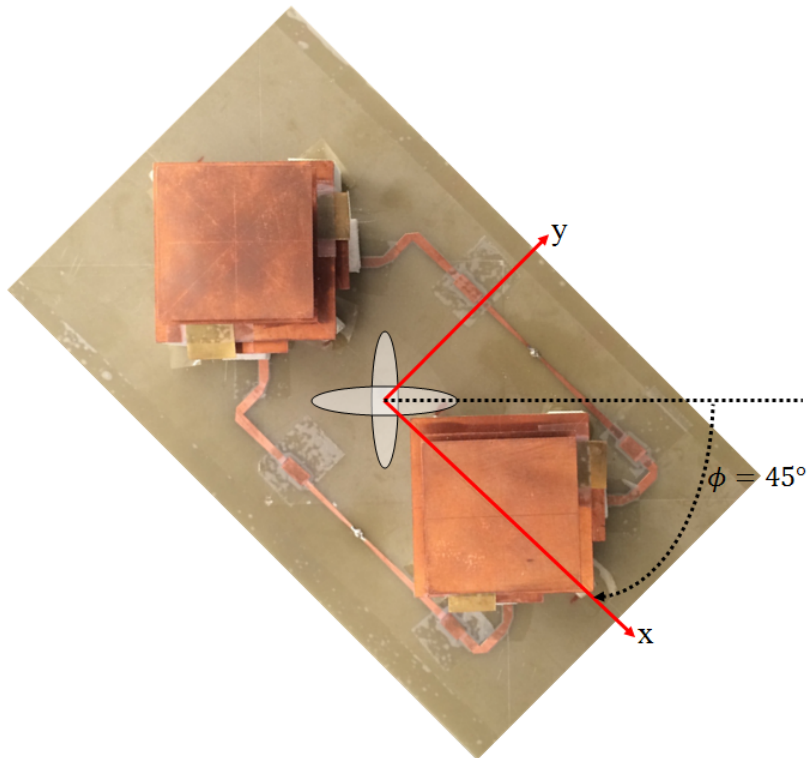
(b) at $\phi=+45°$

Figure 4.7: Two-Element Array Structure with Probe Projections

considered. It is seen in Fig.4.8 that, the simulated and measured radiation patterns are in a good agreement for given frequencies except a slight shift. This shift between measured and simulated radiation pattern may be because of measurement of dimensional errors. According to the alignment with measurement setup, E_ϕ and E_θ at $\phi=0°$ and $90°$ are not the data that enable us to discuss about co-polarization and cross-polarization. However, in order to deal with that, a simple rotation trick is applied, as shown in Fig.4.7b. After that, receiver probe and feeds are aligned and this yields to talk about co-polarization

and cross-polarization.

(a) 1700 MHz
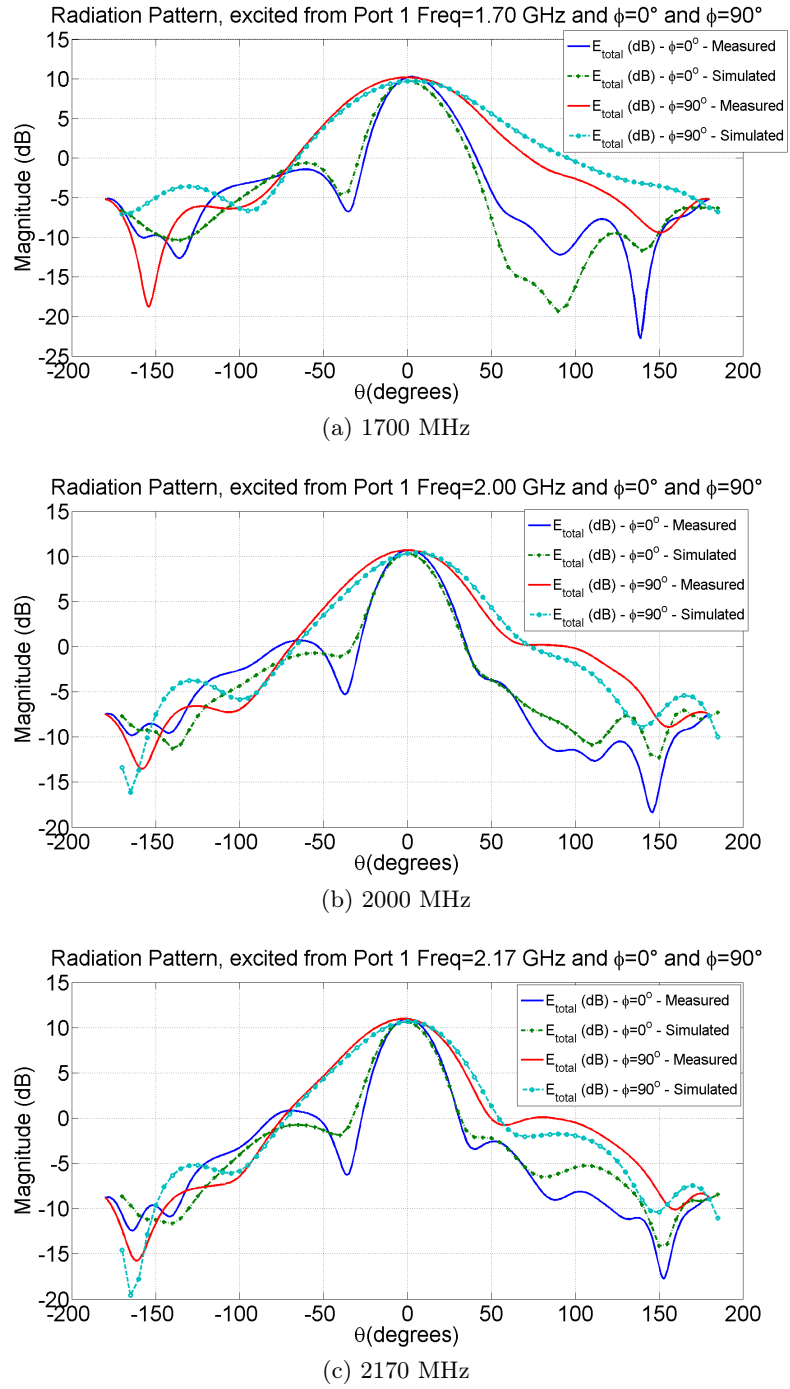
(b) 2000 MHz

(c) 2170 MHz

Figure 4.8: E$_{total}$ at ϕ=0° and 90° for 1700 MHz, 2000 MHz and 2170 MHz

The measurement data of E$_\phi$, E$_\theta$ and E$_{total}$ at ϕ=45° and 135° for 2000 MHz are presented in Fig.4.9 and 4.10.

Radiation Pattern, excited from Port 1 Freq=2.00 GHz and ϕ=45°

(a) ϕ=45°

Radiation Pattern, excited from Port 1 Freq=2.00 GHz and ϕ=135°

(b) ϕ=135°
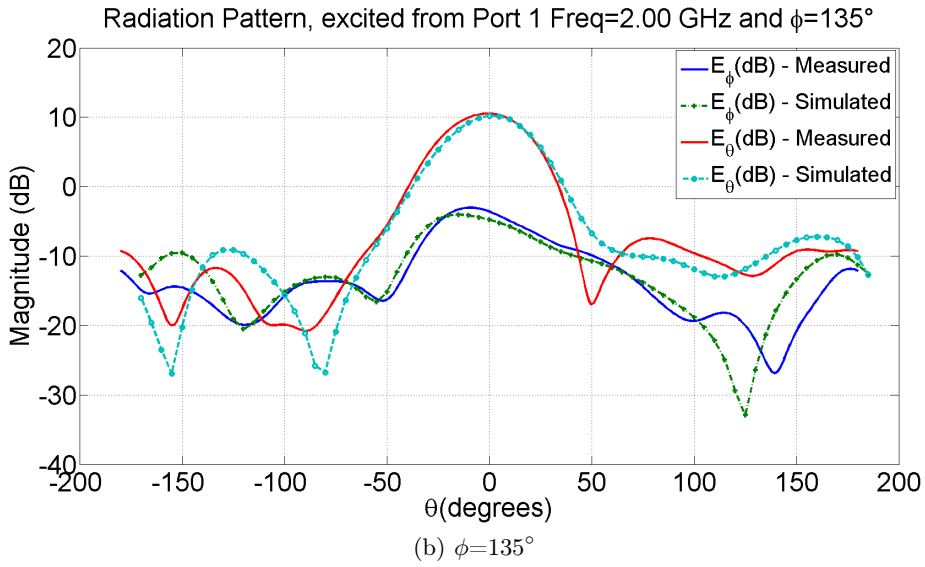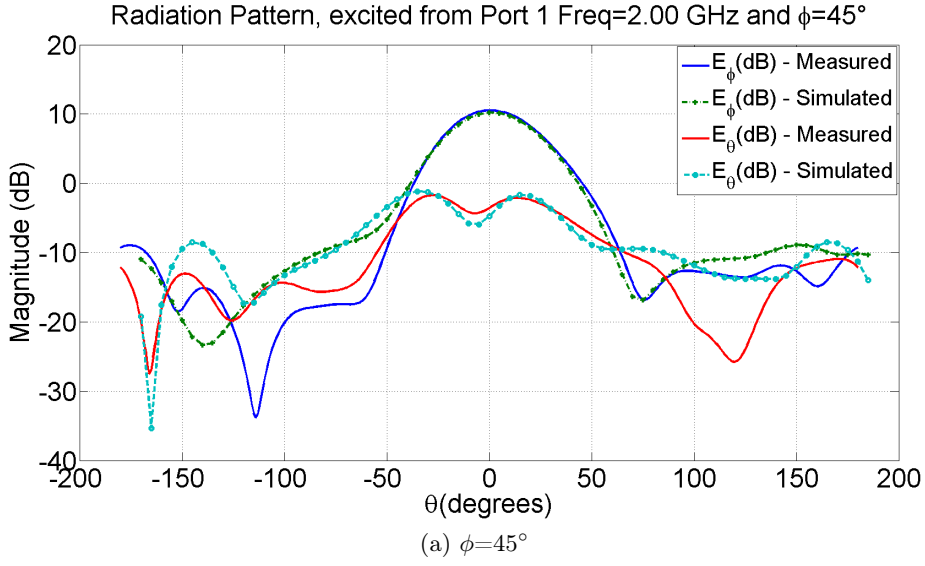
Figure 4.9: E_ϕ, E_θ and E_{total} when array is excited from Port 1 at ϕ=45° and 135° for 2000 MHz

As expected, it is seen that at ϕ=45°, Fig. 4.9a and 4.10a, co-polarization is related with E_ϕ for Port 1 and E_θ for Port 2, and cross-polarization is opposite in port vise, E_θ for Port 1 and E_ϕ for Port 2. In addition to this, it is observed that cross-polarization suppression is more than 15 dB at 2000 MHz. Besides, it is also observed that measured and simulated radiation patterns for excitation from both port 1 and port 2 have nearly the same characteristics around broadside direction of the antenna. However, when the analysis frequencies are set below 1700 MHz or above 2170 MHz, degradations in co-polarization and cross-polarization patterns are observed, as in Fig.4.11.

(a) $\phi=45°$

(b) $\phi=135°$
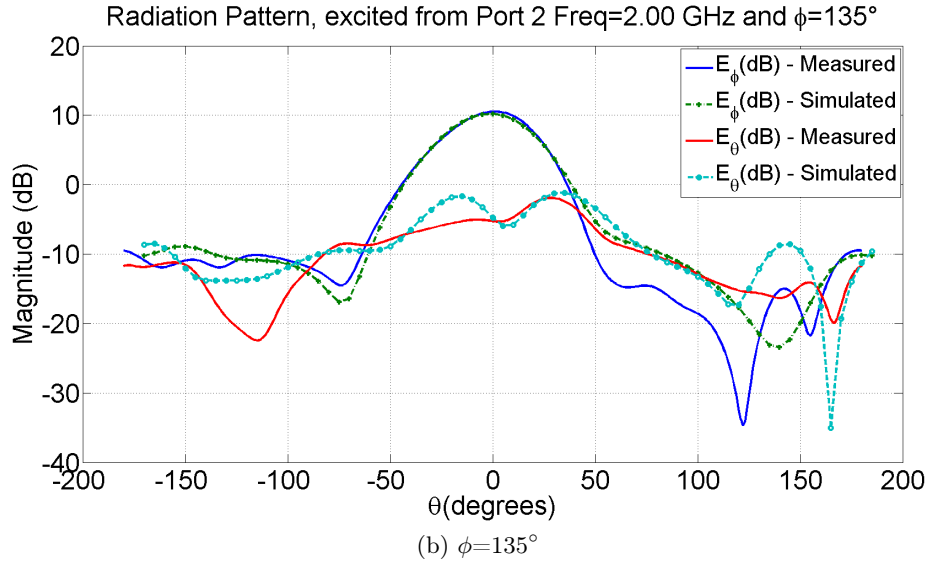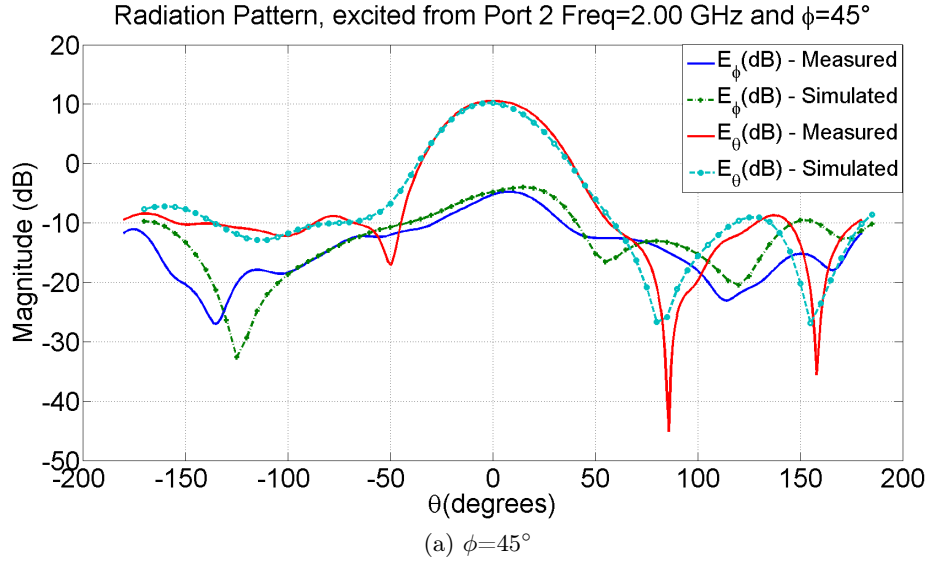
Figure 4.10: E_ϕ, E_θ and E_{total} when array is excited from Port 2 at $\phi=45°$ and $135°$ for 2000 MHz

As it is seen in Fig.4.11b, which is for higher frequency(2500 MHz), around θ=-25°, co-polarized component drops and cross-polarized component dominates. Note that, the excitation of cross-polar component at 2300 MHz was also observed in the simulation results. This was attributed to the radiation of the feed structure that becomes more dominant at frequencies closer to the resonance frequency of the feeding structure. This is generally an unwanted situation for polarization sensitive applications, such as data transfers from both polarization for bandwidth enhancement. This means that, when you receive data from θ=-25°, especially it belongs to the other polarization. As a result, this
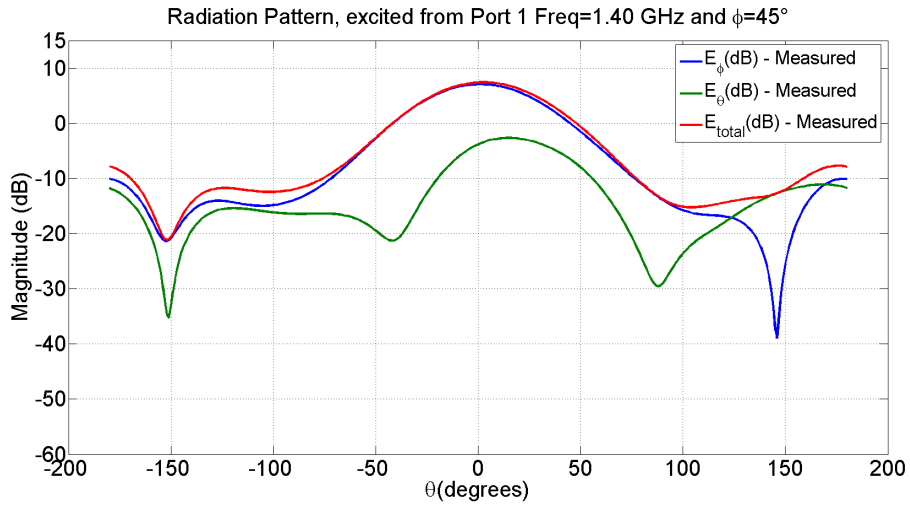
(a) 1400 MHz
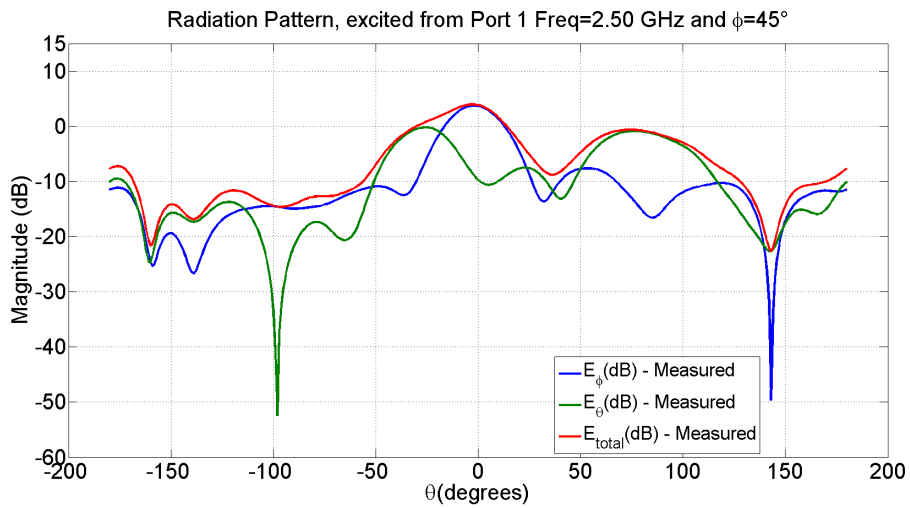
(b) 2500 MHz

Figure 4.11: Pattern and Cross-Polarization Degradation for 1400 MHz and 2500 MHz

cross-polarization is related with this antenna structure and should be carefully investigated when considering the use of this structure in polarization sensitive wireless communication systems.

CHAPTER 5

CONCLUSIONS

In this thesis, analysis and design of a dual polarized wideband microstrip patch antenna, which is electromagnetically excited with elevated wide strips, are studied. The main objective of this thesis is to understand the effects of antenna parameters to the input impedance and the radiation performance of the antenna and provide a guideline to guide antenna engineers for designing similar antennas.

In Chapter 2, an example of an air filled patch antenna excited with an elevated strip is investigated and optimum design parameters are achieved with parametric analysis. The effects of antenna parameters on input impedance bandwidth, as well as return loss, are examined. For the optimized antenna structure, %54 impedance bandwidth is achieved. From these examinations, a proper guideline to obtain initial design parameters for the antenna type, which is used in this study, is presented. The demonstration of this guideline stated in this chapter for a different frequency band is provided. The design guideline is followed step-by-step and the desired antenna design parameters are obtained for 3 GHz - 5 GHz frequency band. It is shown that, for a given proper frequency band, the antenna design parameters could be obtained from the guideline provided. Design and the simulation of a new antenna is done and corresponding results are reported. According to the results, it is shown that %53.6 input impedance bandwidth is achieved. However, it is seen that in order to get the desired impedance bandwidth, tuning of the parameters needs to be done.

In Chapter3, in addition to the Chapter 2, the ability of designing a dual po-

larized antenna structure is demonstrated. Effects of the orthogonal feed on isolation between two ports are examined. It is seen that, by introducing second port, there occurs %10.4 input impedance bandwidth enhancement, which is improved from %54 to %64.4. However, due to the second port, isolation between two ports is also taken into account for better results. In this chapter, it is also observed that, without any precaution, isolation between two ports within the operating band would be insufficient. Therefore, in order to increase the isolation level between two ports, an isolation wall is placed. It is seen that, by the help of this metallic blade, a considerable amount of improvement in isolation level is achieved. However, even though the isolation wall is placed between two ports, the level of isolation within the operating band is still insufficient. In order to increase the isolation between ports, there should be some additional techniques used, which are demonstrated and reported in Chapter 4. Besides, in this chapter the effects of stacked patches on impedance bandwidth, radiation efficiency and radiation pattern is also examined. For this particular analysis, it is seen that even though the overall characteristics of return loss has changed as the number of stacks increases, impedance bandwidth of for a given threshold value, -10 dB, is not affected so much. However, it is observed that as the number of stacked patches increases, isolation between two ports gets better, which is approximately %17 isolation bandwidth improvement with respect to single patch configuration. Additionally, it can be said that no significant effect of additional parasitic patches are observed on the radiation characteristics.

Finally in Chapter 4, a two element array, formed by using dual polarized stacked patches are measured and comparison of simulation and measurement results is made. It is observed that, in lower frequencies, the return loss behavior is very similar for measurement and simulation data for array geometry. However, it is seen that as frequency gets higher simulation and measurement data takes apart from each other, but for a single element case, the return loss characteristic of simulation data is almost same as the measurement data. Besides, co-polarized and cross-polarized components are also examined from the measurement data, which obtained from a near field scanner. It is seen that, the cross-polarization suppression is more than 15 dB around 2 GHz. However, it is observed that as

the frequency gets higher(i.e. 2.5 GHz), the cross-polarized component dominates the co-polarized component within the desired beam-width region. For this type of degradation, it is noted that this should be carefully investigated when considering the use of this structure in polarization sensitive applications.

REFERENCES

[1] Yong-Xin Guo, Kwai-Man Luk, and K-F Lee. L-probe fed thick-substrate patch antenna mounted on a finite ground plane. *Antennas and Propagation, IEEE Transactions on*, 51(8):1955–1963, 2003.

[2] Naftali Herscovici. New considerations in the design of microstrip antennas. *Antennas and Propagation, IEEE Transactions on*, 46(6):807–812, 1998.

[3] Naftali Herscovici. A wide-band single-layer patch antenna. *Antennas and Propagation, IEEE Transactions on*, 46(4):471–474, 1998.

[4] Mustafa Secmen and Altunkan Hizal. An inverted l-shape fed microstrip patch antenna for mobile communication. In *Personal Indoor and Mobile Radio Communications (PIMRC), 2010 IEEE 21st International Symposium on*, pages 1102–1106. IEEE, 2010.

[5] Kin-Lu Wong. *Compact and broadband microstrip antennas*, volume 168. John Wiley & Sons, 2004.

[6] F Croq and A Papiernik. Large bandwidth aperture-coupled microstrip antenna. *Electronics Letters*, 26(16):1293–1294, 1990.

[7] SD Targonski, RB Waterhouse, and DM Pozar. Design of wide-band aperture-stacked patch microstrip antennas. *Antennas and Propagation, IEEE Transactions on*, 46(9):1245–1251, 1998.

[8] Shi-Chang Gao, Le-Wei Li, Mook-Seng Leong, and Tat-Soon Yeo. Dual-polarized slot-coupled planar antenna with wide bandwidth. *Antennas and Propagation, IEEE Transactions on*, 51(3):441–448, 2003.

[9] Hang Wong, Ka-Leung Lau, and Kwai-Man Luk. Design of dual-polarized l-probe patch antenna arrays with high isolation. *Antennas and Propagation, IEEE Transactions on*, 52(1):45–52, 2004.

[10] David M Pozar. *Microwave engineering.* John Wiley & Sons, 2009.

[11] SB Chakrabarty, F Klefenz, and A Dreher. Dual polarized wide-band stacked microstrip antenna with aperture coupling for sar applications. In *Antennas and Propagation Society International Symposium, 2000. IEEE*, volume 4, pages 2216–2219. IEEE, 2000.

[12] AA Serra, P Nepa, G Manara, G Tribellini, and S Cioci. A wideband dual-polarized stacked patch antenna for base stations. In *Antennas and Propagation Society International Symposium 2006, IEEE*, pages 3739–3742. IEEE, 2006.

[13] Vinod K Singh, Zakir Ali, and Ashutosh Kumar Singh. Dual wideband stacked patch antenna for wimax and wlan applications. In *Computational Intelligence and Communication Networks (CICN), 2011 International Conference on*, pages 315–318. IEEE, 2011.

[14] Steven Gao and Alistair Sambell. Dual-polarized broad-band microstrip antennas fed by proximity coupling. *Antennas and Propagation, IEEE Transactions on*, 53(1):526–530, 2005.

[15] Wayne ST Rowe and Rod B Waterhouse. Investigation into the performance of proximity coupled stacked patches. *Antennas and Propagation, IEEE Transactions on*, 54(6):1693–1698, 2006.

[16] WST Rowe and RB Waterhouse. Investigation of proximity coupled antenna structures. In *Antennas and Propagation Society International Symposium, 2003. IEEE*, volume 2, pages 904–907. IEEE, 2003.

[17] Dan Sun and Lizhi You. A broadband impedance matching method for proximity-coupled microstrip antenna. *Antennas and Propagation, IEEE Transactions on*, 58(4):1392–1397, 2010.

[18] Anil B Nandgaonkar and Shankar B Deosarkar. Broadband stacked patch antenna for bluetooth applications. *Journal of Microwaves, Optoelectronics and Electromagnetic Application*, 8(1):1–5, 2009.

[19] Zarreen Aijaz and SC Shrivastava. Coupling effects of aperture coupled microstrip antenna. *Internal Journal of Engineering Trends and Technology, July-August*, (2011).

[20] P Agrawal and MC Bailey. An analysis technique for microstrip antennas. *Antennas and Propagation, IEEE Transactions on*, 25(6):756–759, 1977.

[21] Stuart A Long and Mark D Walton. A dual-frequency stacked circular-disc antenna. *IEEE Transactions on Antennas and propagation*, 27:270–273, 1979.

[22] WFYT Richards, Yuen Lo, and D Harrison. An improved theory for microstrip antennas and applications. *Antennas and Propagation, IEEE Transactions on*, 29(1):38–46, 1981.

[23] MD Deshpande and MC Bailey. Input impedance of microstrip antennas. *Antennas and Propagation, IEEE Transactions on*, 30(4):645–650, 1982.

[24] David M Pozar. Input impedance and mutual coupling of rectangular microstrip antennas. *Antennas and Propagation, IEEE Transactions on*, 30(6):1191–1196, 1982.

[25] Albert Sabban. A new broadband stacked two-layer microstrip antenna. In *Antennas and Propagation Society International Symposium, 1983*, volume 21, pages 63–66. IEEE, 1983.

[26] RQ Lee, KF Lee, and J Bobinchak. Characteristics of a two-layer electromagnetically coupled rectangular patch antenna. *Electronics letters*, 23(20):1070–1072, 1987.

[27] N Montgomery. Triple-frequency stacked microstrip element. In *Antennas and Propagation Society International Symposium, 1984*, volume 22, pages 255–258. IEEE, 1984.

[28] Daniel H Schaubert, David M Pozar, and Andrew Adrian. Effect of microstrip antenna substrate thickness and permittivity: comparison of theories with experiment. *Antennas and Propagation, IEEE Transactions on*, 37(6):677–682, 1989.